





Review

# A Critical Review on Battery Aging and State Estimation Technologies of Lithium-Ion Batteries: Prospects and Issues

Probir Kumar Roy <sup>1</sup>, Mohammad Shahjalal <sup>2</sup>, Tamanna Shams <sup>3</sup>, Ashley Fly <sup>4</sup> , Stoyan Stoyanov <sup>2</sup> , Mominul Ahsan <sup>5,\*</sup>  and Julfikar Haider <sup>6</sup> 

<sup>1</sup> Department of Electronics and Electrical Engineering, Chittagong University of Engineering and Technology, Chattogram 4349, Bangladesh; probirrooy1702085@gmail.com

<sup>2</sup> Old Royal Naval College, University of Greenwich, Park Row, London SE10 9LS, UK; mshahjalal2024@gmail.com (M.S.); s.stoyanov@greenwich.ac.uk (S.S.)

<sup>3</sup> Department of Physics, University of Dhaka, Dhaka 1000, Bangladesh; tamannaduph@gmail.com

<sup>4</sup> Department of Aeronautical and Automotive Engineering, Loughborough University, Loughborough LE11 3TU, UK; a.fly@lboro.ac.uk

<sup>5</sup> Department of Computer Science, University of York, Deramore Lane, York YO10 5GH, UK

<sup>6</sup> Department of Engineering, Manchester Metropolitan University, John Dalton Building, Chester Street, Manchester M1 5GD, UK; j.haider@mmu.ac.uk

\* Correspondence: mominul.ahsan2@gmail.com

**Abstract:** Electric vehicles (EVs) have had a meteoric rise in acceptance in recent decades due to mounting worries about greenhouse gas emissions, global warming, and the depletion of fossil resource supplies because of their superior efficiency and performance. EVs have now gained widespread acceptance in the automobile industry as the most viable alternative for decreasing CO<sub>2</sub> production. The battery is an integral ingredient of electric vehicles, and the battery management system (BMS) acts as a bridge between them. The goal of this work is to give a brief review of certain key BMS technologies, including state estimation, aging characterization methodologies, and the aging process. The consequences of battery aging limit its capacity and arise whether the battery is used or not, which is a significant downside in real-world operation. That is why this paper presents a wide range of recent research on Li-ion battery aging processes, including estimations from multiple areas. Afterward, various battery state indicators are thoroughly explained. This work will assist in defining new relevant domains and constructing commercial models and play a critical role in future research in this expanding area by providing a clear picture of the present status of estimating techniques of the major state indicators of Li-ion batteries.

**Keywords:** battery management system (BMS); state estimation; aging characterization methodology; battery aging; Li-ion battery; state of function (SOF); state of power (SOP); state of health (SOH); state of charge (SOC)



**Citation:** Roy, P.K.; Shahjalal, M.; Shams, T.; Fly, A.; Stoyanov, S.; Ahsan, M.; Haider, J. A Critical Review on Battery Aging and State Estimation Technologies of Lithium-Ion Batteries: Prospects and Issues. *Electronics* **2023**, *12*, 4105. <https://doi.org/10.3390/electronics12194105>

Academic Editor: Yi-Hua Liu

Received: 14 August 2023

Revised: 24 September 2023

Accepted: 27 September 2023

Published: 30 September 2023



**Copyright:** © 2023 by the authors. Licensee MDPI, Basel, Switzerland. This article is an open access article distributed under the terms and conditions of the Creative Commons Attribution (CC BY) license (<https://creativecommons.org/licenses/by/4.0/>).

## 1. Introduction

In the contemporary context of global decarbonization efforts, the robust advancement and integration of renewable energy sources emerge as an inexorable trajectory. Nonetheless, the inherent intermittency of many renewables introduces temporal and spatial disparities between energy generation and end-user consumption. To effectively bridge these gaps, the imperative arises to cultivate tailored energy storage systems optimized for the demands of the modern power grid [1]. During the 1980s, the development of lithium-ion batteries (LIBs), as documented in references [2–4], marked a significant milestone in electrochemical energy storage systems. LIBs distinguished themselves from other commercially available battery types by offering substantial advantages, including extended cycle life, elevated working voltage, and impressive specific energy [5]. Battery management systems (BMSs) are required to meet more stringent requirements in order to

improve LIB utilization. These requirements include all-climate, electric scopes, full lifetimes, and high-precision battery state estimates such as safety status, fault, state of health (SOH), and state of charge (SOC). For the development of new high-energy vehicles, as well as energy conservation and emission reduction strategies, comprehensive investigations are a must. As a result, it is critical to take advantage of a more mature and comprehensive BMS [6–9]. The BMS should minimize the total cost of a vehicle by not only ensuring the battery pack's safe functioning [10,11] but also fully using the pack's available energy and extending durability [12]. However, the current charging strategies for Li-ion batteries in EVs have severely limited their widespread adoption [13,14]. To solve this problem, research into providing an optimum charging method for Li-ion batteries has arisen as a new paradigm for a smarter BMS [15,16]. The SOH of each cell in the system is strongly related to the creation of the optimal charging technique for a Li-ion battery pack in an EV [17–19], which poses substantial challenges [12,20,21].

It is necessary to investigate the battery aging process and deterioration model at the cell level, particularly how battery essential factors affect battery life and other important characteristic metrics like power and energy density. The aging process and deterioration model are also crucial at the battery system level. In terms of battery management for estimating battery health based on history, optimizing current working conditions, and estimating future performance, Vetter et al. [22] provide an in-depth analysis of the aging mechanisms of LIBs with lithium metal oxide cathodes (lithium nickel cobalt mixed oxides [Li(Ni,Co)O<sub>2</sub>]) and lithium manganese oxides [LiMn<sub>2</sub>O<sub>4</sub>]) and carbonaceous anodes. Han et al. [23] offer a thorough examination of the fundamental problems surrounding battery degradation during its entire life cycle. Li et al. [24] provide a thorough examination of one common aging mechanism: lithium deposition. Santhanagopalan et al. [25] provide an overview of models for forecasting LIB cycling performance. Wang et al. [26] discuss the modeling of solid electrolyte interface (SEI) films in detail. Different approaches are outlined in [27], ranging from an electrochemical perspective to research that is specifically focused on data processing, to comprehend the effects of aging mechanisms on a battery's life. In reference [28], a rapid identification methodology is introduced for assessing micro-health parameters that characterize the performance of LiFePO<sub>4</sub> negative electrode materials and electrolytes. This approach is rooted in the reduced P2D model and employs Páde approximation techniques. To facilitate micro-health parameter determination, the diffusion processes within the P2D model's liquid phase and solid phase are individually simplified using the Páde approximation method. Farmann et al. [29] and Berecibar et al. [30] provide crucial assessments of the battery SOH estimate techniques, with an emphasis on the management method. In battery behavior analysis, battery state tracking, real-time controller design, and thermal management, a good battery model is essential. Furthermore, certain internal battery states, such as the state of charge (SOC), state of health (SOH), and internal temperature, cannot be directly evaluated despite the fact that these states play critical roles in maintaining battery operation and must be controlled using appropriate estimating techniques. Various methods are reported in the literature in this respect. A review of the strengths and weaknesses of SOC estimating methods for LIBs in electric and hybrid electric vehicles (HEVs) was published in reference [31], with 65 percent of references dating from 2011 or earlier. In reference [32], an innovative approach is presented for jointly estimating the state of charge (SOC) and temperature of a lithium iron phosphate battery. This method utilizes ultrasonic reflection waves, employing a piezoelectric transducer affixed to the battery's surface for ultrasonic-to-electric transduction. Ultrasonic signals are generated at the transducer, traverse through the battery, and return to the transducer after reaching the battery's underside. The intervals for extracting feature indicators of the battery's state are determined through sliding-window matching correlation analysis. Experimental results demonstrate that the root mean square error (RMSE) for estimating the lithium-ion battery's SOC is 7.42%, while the temperature estimation yields an RMSE of 0.40 °C. Reference [33] provides a review of management systems and electric vehicle applications, with an emphasis on the estimation method of the state of charge rather than the estimation

methods of the state of health and state of function. More than half of the citations in this literature date from 2012 or earlier. Many key methods are not explained in reference [12], such as the genetic-algorithm-based method, adaptive unscented Kalman filter (AUKF), sigma-point Kalman filter (SPKF), and so on. Furthermore, the state-of-function technique discussed in this literature is solely based on the SOC and SOH.

In contrast to references [34–36], which predominantly focus on specific aspects such as the state of health (SOH) or battery performance measurement, this paper offers a comprehensive review that encompasses a wider array of topics. It delves into battery aging mechanisms, their origins, techniques for battery state estimation, and various related subjects. Our paper offers a unique perspective by concurrently reviewing state estimation parameters such as the state of charge, state of health, state of function, state of temperature, and state of power, alongside an in-depth exploration of battery aging mechanisms. This comprehensive approach distinguishes our work from other review papers and provides valuable insights to assist battery management system designers in their endeavors. The rest of this paper is structured as follows. Section 2 details the aging process of LIBs. Section 3 depicts the state estimation procedure. In Section 4, the future research path is stated. Section 5 contains the conclusion.

## 2. Aging Mechanism

### 2.1. General Aspects

How effectively the battery aging mechanisms and their consequences are studied and analytically expressed determines the performance of health estimates and the accuracy of predictions [37]. A metal oxide cathode, a carbonaceous anode, a lithium salt electrolyte, and a separator are the principal components of a LIB. The main cause of battery aging is the physiochemical transformation that takes place within the electrolyte, electrode, and the interfaces between them. The origins of aging mechanisms are heavily influenced by the composition of the electrodes. Aging causes cell component degradation. This may lead to structural modifications, alterations in the electrolyte's chemical makeup, or a loss of active material as a result of materials dissolving in the electrolyte [22]. Figure 1 [38] depicts the various kinds of aging mechanisms that occur in LIBs.

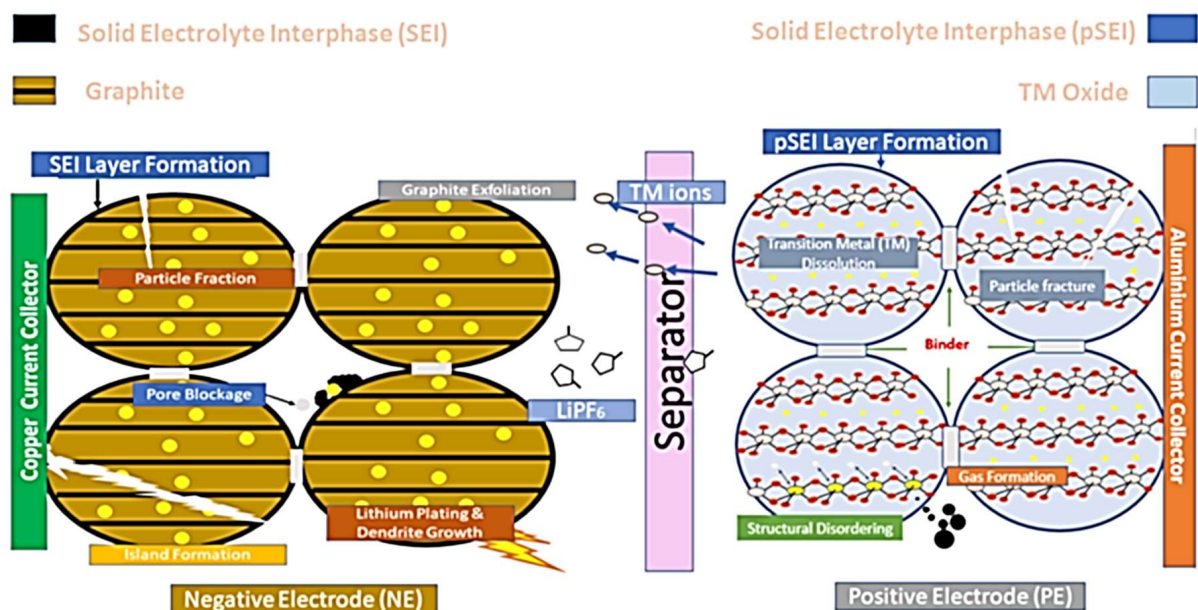


**Figure 1.** The most significant Li-ion battery degrading mechanism is summarized graphically (adapted from [38]).

There are three different modes of the main degradation mechanisms in Li-ion batteries: the loss of anode/cathode active material (LAM) in the electrodes, loss of lithium inventory

(LLI), and growth in cell internal resistance. LLI groups the side reactions that limit how much cyclable lithium is available to transfer between electrodes, for instance, the surface of the negative electrode developing a solid electrolyte interface (SEI), lithium plating, or electrolyte decomposing reactions [27]. Such reactions degrade Li ions in an irreversible manner, rendering them unavailable for further discharge/charge. The LAM refers to a group of mechanisms that reduce the amount of material accessible for electrochemical activities in both anode and cathode electrodes. The LAM usually occurs for several different reasons. One of the reasons is the structural degradation of electrodes caused by active material volume changes during cycling. These cause particles to crack and lower the density of lithium storage sites by causing mechanical stress. Chemical breakdown and dissolving processes of transition metals into the electrolyte, as well as SEI alteration, are other viable reasons [27,39]. At the junction of the two electrodes, there is an electrolyte loss (LE), because of parasitic phases such as SEI formation, and various mechanisms such as lithium plating, high temperature, and high voltages, with moisture intrusion leading to the production of hydrofluoric acid (HF), can cause the cell's resistance to increase [38].

### 2.1.1. Mechanisms of Anode Material Aging

Carbonaceous anodes, which are primarily graphite-based materials, are presently used in the majority of commercial LIBs. The primary mechanism for graphite electrodes to age over time is the development of a passivation protective layer interface, also known as the SEI, on the surfaces of the anode electrode during the discharging/charging operation [40] at voltages below the electrolyte's electrochemical stability window. This causes irreversible redox reactions to break down the electrolyte, resulting in electrolyte losses. The SEI layer develops on its own during the first cycle, leading to ca. 10% loss in capacity, but it then functions to block additional electrolyte reactivity at the negative electrode (NE). The SEI obstructs the reactions that occur between the electrolyte and the electrode in general. However, as the cell ages, the thickness of the SEI layer grows (mostly on the graphite NE) because of a volume change of the graphite anode material of around 10% for lithium ions intercalation and deintercalation during battery charging/discharging. An SEI is created by the reaction of the electrolyte and side reaction products, such as plated lithium ions and transition metal (TM) ions dissolved from the positive electrode (PE), with solvent molecules passing through the already-existing SEI, and newly exposed electrode surfaces as a result of cracking and deposition of these products could contribute to the thickening of the SEI layer [38]. This causes the battery's usable capacity to decrease with time, as well as the internal resistance of the battery to rise [23,37,41]. One of the key causes of LIB aging is the development and continuing thickening of the SEI layer on the surface of the graphite anode [42]. The SEI grows at a rate roughly proportional to the square root of time, and as the SEI gets thicker, the rate at which solvent molecules diffuse into the SEI decreases [38].

The formation of the SEI in a Li-ion battery involves several steps. When compared to the  $\text{Li}^+/\text{Li}$  reduction potential, the first stage happens at voltages greater than 0.25 V [43]. In the first step, electrolyte decomposition begins through a series of reduction reactions, as well as the formation of insoluble compounds ( $\text{Li}_2\text{O}$ ,  $\text{LiF}$ , and  $\text{Li}_2\text{CO}_3$ ) [43]. The second stage begins between 0.25 and 0.04 V where the graphite electrode has intercalated Li ions [43]. Storage and operation at high temperatures can cause the SEI layer to dissolve, resulting in the formation of salts that are less permeable to  $\text{Li}^+$  ions [27]. At low temperatures, lithium plating, higher impedance, and more cyclable lithium losses might arise from lower lithium diffusion inside the SEI and graphite [27]. Exfoliation and gas evolution are caused by the interaction of solvents that disperse through the SEI and the graphite electrode, which can damage the SEI [39]. Increased impedance and capacity loss can also be caused by cracks in the SEI [41]. This kind of depreciation can be reduced by keeping batteries at lower voltages [27]. The high-voltage-induced SEI layer on the cathode is responsible for the formation of an SEI, electrolyte degradation, electrolyte oxidation, and active mass wear, which is difficult to detect [44].



When metallic Li develops on the NE's surface rather than intercalating into it, a phenomenon known as "Li plating" takes place, which is another cause of battery degradation. This can be caused by quick charge, when the side reaction rate is raised compared to the main intercalation reaction (kinetic plating) for high electrolyte potential [45], or by the NE surface becoming fully lithiated, in which case the Li has nowhere else to go (thermodynamic plating) [38,46]. There are several causes of lithium plating, such as high cell voltage, high (charge) current, high SOC, low temperatures, and a lack of NE mass or electrochemically active surface area. Furthermore, plating for local faults is caused by manufacturing defects [47] or application errors [48]. The plated metallic Li immediately reacts with the electrolyte to develop the SEI shown in Figure 2 [38], resulting in the isolation of the remaining Li and the development of "dead lithium" [38,49–51]. As a result, pore blockage causes conductivity reduction [49]. Puncturing the separator for dendrite formation owing to an internal short circuit may result from metallic lithium plating [38,52].

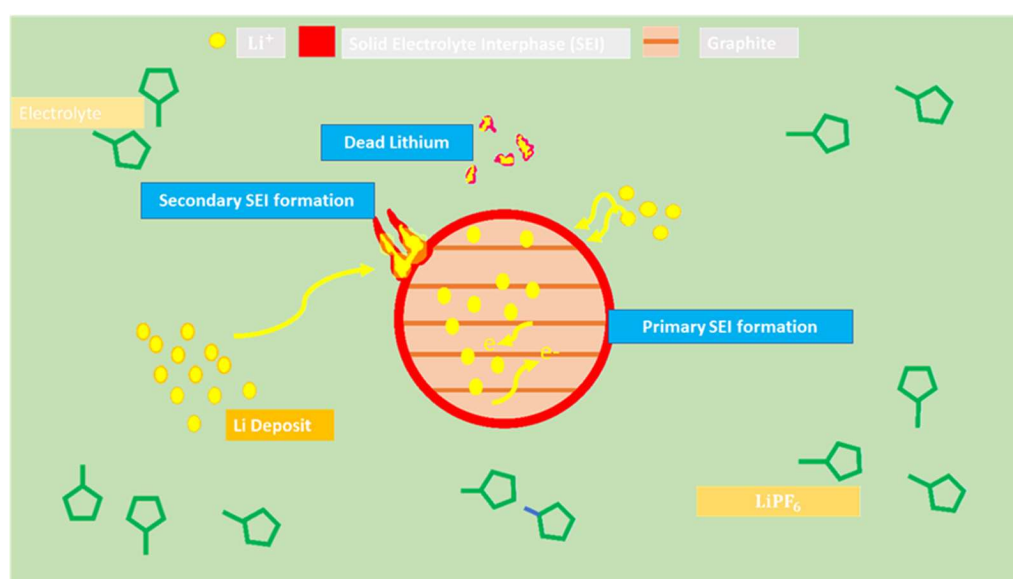


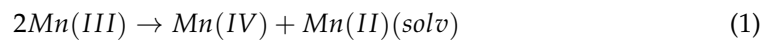
**Figure 2.** Correlation between the solid electrolyte interface (SEI) and lithium plating (adapted from [38]).

Particle fracture occurs in both electrodes as a result of the significant volume change in the electrode materials and the resulting stress during electrochemical operation [53]. Particle breakage is particularly problematic for active materials like silicon that have high theoretical specific capacitance. In addition to permitting side reactions to occur, electrode particle cracks reveal extra electron-conductive surfaces to liquid electrolytes, trapping Li that would otherwise be cyclable [54] inside of the enlarged SEI layer. Particle fracturing and the related protracted SEI expansion are more possible in NEs with a high Si concentration because they are subjected to more dramatic volume fluctuations during cycling [55]. The cracking of particles has a multitude of repercussions. Active particles lose electrical contact with the current collector, conductive additives, and current collector. As a result, electronic/ionic conductivity declines, and capacity fades [38,54,56]. The rate of SEI development has also risen, contributing to capacity fading. Electrode pulverization is the process by which some of the active material separates from the remainder of the particle when microscopic cracks in the electrode join together [38]. As a result, there is a loss of active material, which causes capacity fading [38].

### 2.1.2. Mechanisms of Anode Material Aging

The main challenges related to battery aging for metal oxide cathodes are electrode material dissolution, electrode structural deterioration, and phase shift. As a result, cathode dissolution can exacerbate electrolyte deterioration, resulting in the passive layer at the

cathode/electrolyte interface expanding continuously. Depending on the electrode material, the degree of dissolution varies [57]. In general, Mn-based cathode dissolution is expected to be the most intense [58,59], whereas Ni-based cathode dissolution is considered to be the least intense [60]. For Mn-based cathodes, Jahn–Teller distortion and manganese dissolving are the two main aging processes that cause structural deformation [23,61,62]. Manganese is often found in two oxidation states:  $Mn^{4+}$  and  $Mn^{3+}$ . During the discharged state, trivalent manganese ions are disproportionately converted to tetravalent and divalent manganese ions in this process [22,63] which is shown in Equation (1).



When discharging at a high current, Li ions diffuse much more quickly in the electrolyte than in LMO particles, resulting in Li ions building up on the surface of the LMO particles. LMO spinel may also saturate with additional lithium, which results in Jahn–Teller distortion and a phase transition from cubic to tetragonal. Since the cathode material's structure is disrupted and the volume of the LMO cathode material fluctuates significantly (by around 16%), the active material is lost [23,64,65]. Reference [58] identified two aging processes for Mn-based cathodes: low potential Mn disproportionation and medium and high potential Mn dissolution affected by  $H^+$  with the co-product of LiF, a passive film, known as the cathode electrolyte interface (CEI) film and generally thinner than the SEI film, can form as the electrolyte oxidizes and LiPF<sub>6</sub> decomposes during the initial and successive charging. With more battery cycles, the cathode/electrolyte interface's CEI layer thickens, increasing interface resistance and deepening cathode polarization. Therefore, it can affect the battery's rate capacity and reversible capacity [66]. Lithium vacancies and cation mixing contribute to the structural deterioration of the cathode material. The cation mixing frequently happens at the transition metal cathode because various transition metal ions ( $Ni^{2+}$ ,  $Mn^{3+}$ ,  $Fe^{2+}$ ) and Li ions have similar radii. It can limit battery capacity by preventing certain Li ions from intercalating, as well as widen the interlayer gap of the transition metal layer, preventing Li ion diffusion and raising battery polarization. Lithium vacancies would arise in LiCoO<sub>2</sub> cathodes due to the smaller radius of  $Co^{2+}$ , making structures unstable. Particle breaking on the PE, similar to the behavior witnessed at the NE, might expose new surfaces to electrolytes, thus increasing the degrading processes. Dissolved TM ions can move to the NE through the electrolyte [67–69], producing deposits that can promote the creation of thicker, layered SEI structures, thereby raising NE impedance [12,38,66].

## 2.2. Origins of Aging

The two forms of battery aging are cycle aging and calendar aging [70]. Calendar aging is the term for the harm that happens as a result of battery storage over time [71]. As a result, depending on the storage conditions, battery activities may be sped up or slowed down. The impact of the battery operation interval known as a cycle is connected to cycle aging (discharge or charge).

The storage temperature [72] is the most important factor when it comes to self-discharge and calendar aging. High temperatures accelerate secondary processes like corrosion, and lithium loss is higher than at low temperatures, which causes capacity fading [72,73]. Low temperatures prevent these processes from happening as quickly, but they also generate problems because of material loss and chemical alterations [11]. The amount of the SOC during storage [27,74] is another important element in calendar aging. According to Bashash et al. [75], there is an exponential relationship between an increased SOC and a higher rate of calendar aging. As a result, if the battery is stored at high SOCs, it will degrade faster. The power law connection between time  $t$  and the loss of calendar aging capacity is weighted by the effects of storage SOC and temperature  $t$ , which may be caused by a stress factor  $k_{cal}$  [76].

$$Q_{loss}^{cal}(t) = Q(t) - Q(0) = k_{cal}(T, SOC)t^{z_{cal}} \quad (2)$$

where  $Q_{loss}^{cal}(t)$  is a measure of the capacity loss that occurs during calendar aging. The cell capacity at time  $t$  and at its beginning of life (BOL), respectively, is represented by  $Q(t)$  and  $Q(0)$ . The constant exponent  $Z_{cal}$  has no dimensions. Temperature  $T$  and SOC have an impact on the value of  $k_{cal}$ .

When the battery is in charge/discharge, cycle aging occurs as a direct result of the average SOC, temperature, cycling voltage range, charge/discharge current rate, and cycle number/time, when cycling. The battery consumption mode determines the parameters that contribute to cycle aging. The  $\Delta SOC$ , which indicates SOC fluctuation during a cycle, is a common factor in the literature. Bloom et al. tested identical lithium-ion cells for varied  $\Delta SOC$  cycling at similar temperatures and beginning SOC. The results reveal power loss increasing with  $\Delta SOC$ . Such effects are primarily caused by positive electrode deterioration and the growth of the SEI, both of which are induced by high charge or discharge. The charging/discharging voltage during the life of a LIB has an influence on its aging and the operation of the usage mode. As a result, a high charging voltage indicates a faster aging process [77]. Cycle-based capacity loss can be expressed as a power law relationship with throughput in a commonly used cycle aging model [41].

$$Q_{loss}^{cyc}(L) = Q(L) - Q(0) = k_{cyc}(T, I, DOD) \cdot L^{z_{cyc}} \tag{3}$$

where  $Q_{loss}^{cyc}$  is a measure of the capacity loss that occurs during cyclic aging and represents the total capacity variation over time/cycles. The cycle number or Ah-throughput are both acceptable values for  $L$  [43].  $I$  represents the cycling current, while  $k_{cyc}$  reflects the impact of aging variables on the deterioration process. DOD stands for the depth of discharge while cycling. Once more, the exponent  $z_{cyc}$  is a constant that was obtained via fitting experimental data [43]. At high SOC values, electrolyte decomposition at the electrode contact surface induces an increase in lithium consumption and the formation of insulating layers on the electrode particle surface, resulting in capacity loss and a rise in impedance [78]. Furthermore, at low SOC values, corrosion of the current collector, which has been recognized as the primary harmful impact, occurs [40]. High charging and discharging rates will reduce the capacity of the cell and increase internal resistance [78]. The high current generates a localized temperature capable of modifying and disrupting the electrode surface layers [22,79,80]. The effects of storage temperature on calendar aging are described in [22,27]. At high temperatures, side reactions increase, resulting in capacity loss [27]. The rate of fading increases as the temperature rises. While the Li-ion diffusion rate in the electrolyte decreases with low-temperature storage, the rate of plating of metallic lithium on the anode increases. That is why capability is depleted. [27]. Table 1 shows external factors influencing battery aging during cycling, as well as their related degradation modes [39].

**Table 1.** External factors affecting battery aging and degradation modes.

Degradation Mechanism	Aging Stress Factors						Degradation Mode			Effect	
	Time	High Temperature	Low Temperature	High SOC/Voltage	Low SOC/Voltage	High Current Rate	High Pressure	LLI	LAM		Increase in Impedance
SEI growth	✓	✓	—	✓	—	✓	✓	✓	—	✓	Capacity fade
SEI decomposition	—	✓	—	✓	—	✓	—	✓	—	—	Capacity fade
Electrolyte decomposition	—	✓	—	✓	—	—	—	✓	✓	✓	Capacity fade
Graphite exfoliation	—	—	—	✓	—	✓	—	—	✓	—	Capacity fade Power fade
Lithium plating/Dendrite formation	—	—	✓	✓	—	✓	—	✓	✓	—	Capacity fade

Table 1. Cont.

Degradation Mechanism	Aging Stress Factors						Degradation Mode				Effect
	Time	High Temperature	Low Temperature	High SOC/Voltage	Low SOC/Voltage	High Current Rate	High Pressure	LLI	LAM	Increase in Impedance	
Loss of electric contact	—	—	—	—	✓	✓	—	—	✓	—	Capacity fade, Power fade
Electrode particle cracking	—	—	—	—	—	✓	✓	—	✓	—	Capacity fade, Power fade
Transition metal dissolution	—	—	—	—	✓	—	—	—	✓	—	Capacity fade, Power fade
Corrosion of current collectors	—	—	—	—	✓	—	—	—	✓	✓	Capacity fade, Power fade

### 3. Battery State Estimation

One of a BMS's most significant features that aid with the interpretation of battery activity is the assessment of the battery's status. A number of metrics or conceptions are developed to measure the battery's state of functioning to assess the aging described below.

#### 3.1. SOC Estimation

The SOC is a measure of how much capacity remains available compared to the battery's full capacity, and it can be calculated using the following formula [81].

$$SOC(t) = \frac{C_p}{C_m} \times 100\% \quad (4)$$

where  $C_p$  denotes the remaining capacity that may be used to power electronics equipment. The maximum accessible capacity that the cell can hold, as defined by the battery's electrochemical properties, is represented as  $C_m$ . The SOC is one of the most critical states that must be controlled to maximize performance and prolong battery life. SOC evaluation is complexly impeded by substantial battery characteristic changes during its lifespan owing to deterioration and distinguished non-linear behavior. As a result, researchers were motivated to suggest numerous approaches that specifically increased difficulties in building a connection between efficiency and procedure robustness. The following are some prominent approaches with features that may be used to identify appropriate evolution techniques and assist researchers in selecting the optimal method for their needs.

##### 3.1.1. Conventional Method

The most common conventional SOC estimation technique is using the battery's OCV. As the SOC is connected with lithiation in a LIB's active material, the OCV may be used to determine the SOC after ample rest for the battery to achieve equilibrium [82]. This approach is simple to use and highly accurate. Under controlled situations (ambient temperature, specified discharge rate), the discharge test was performed, and it was found to be the most accurate way to evaluate the battery SOC [12]. This is a time-consuming process and is only applicable in laboratories. The coulomb counting (CC) technique, which relies on battery current integration throughout time when the battery is charged or discharged, is another method for calculating the SOC. It is a highly effective and easy method, but it is not preferable as a sole estimation method for very complex conditions as current measurement errors will accumulate over time, leading to inaccurate SOC estimation. Systems utilize battery current and voltage to measure the internal resistance. During a short duration (<10 ms) [33], the variation of the current transition determines the voltage. The current and voltage difference ratio causes direct current (DC) resistance reflecting the DC power of a battery. In terms of achieving an understanding, electrochemical impedance



spectroscopy (EIS) has been employed extensively inside the batteries for diagnostics and SOC estimation. EIS uses inductances and capacitances to measure the battery impedance along with a broad frequency range [83]. A battery model is required to obtain the OCV online for estimating the SOC while the vehicle is in use. In the literature, equivalent circuit models (ECMs) [84] and electrochemical models (EChMs) [85–87] are frequently utilized onboard battery models. For simulating battery output, ECMs are commonly used. The Thevenin model (Figure 3a) is one of many ECMs that have been implemented. Due to its RC network form, the Thevenin model has non-linear properties, thereby considering the polarization of the battery’s internal electrochemical reaction. Polarization resistance  $R_p$ , equivalent capacitance  $C_p$ , ohmic resistance  $R_0$ , and OCV are the elements that make up this model. The equations of this model are given below [88].

$$U_L = U_{OCV} - IR_0 - U_P \tag{5}$$

$$U_P = -\frac{1}{C_p R_p} U_P + \frac{1}{C_p} I \tag{6}$$

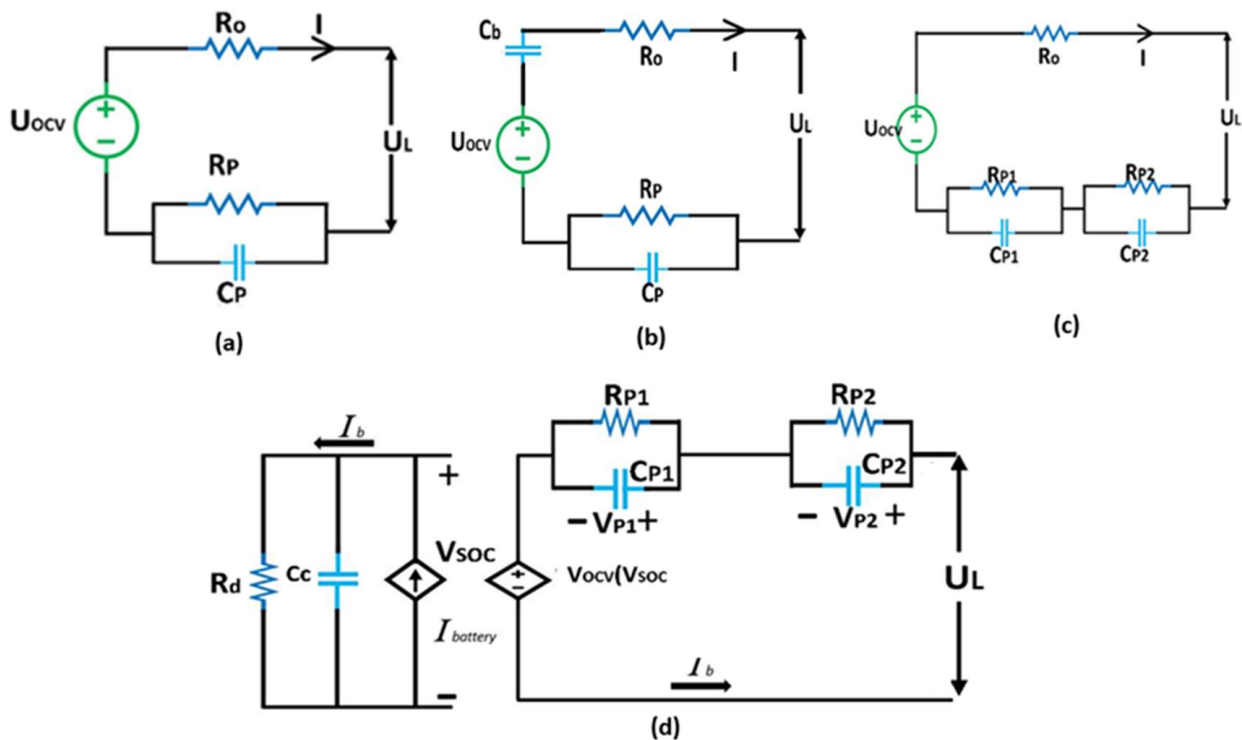


**Figure 3.** Schematic diagram of equivalent circuit models (ECMs) of battery: (a) the Thevenin model, (b) PNGV model, (c) DP model, and (d) source-dependent ECM.

Another model is “The partnership for a new generation of vehicles (PNGV) model” (Figure 3b) that is acquired based on the Thevenin model by adding an equivalent capacitance  $C_b$  to characterize the stored charge capacity and explain how the OCV of the battery varies over time [89]. The model is also called a first-order ECM. The  $C_b$  value represents the battery power level. The model follows the equations [88] below.

$$SU_L = U_{OCV} - IR_0 - U_P - U_{C_b} \tag{7}$$

$$\dot{U}_P = -\frac{1}{C_p R_p} U_P + \frac{1}{C_p} I \tag{8}$$

$$\dot{U}_{C_b} = \frac{1}{C_b} I \quad (9)$$

To simulate concentration and electrochemical polarization, the dual-polarization (DP) model (Figure 3c) or second-order ECM is obtained by including a second RC network into the Thevenin model for improving the estimation of dynamic battery response accuracy. The model can be expressed as below [88].

$$U_L = U_{OCV} - IR_0 - U_{P1} - U_{P2} \quad (10)$$

$$\dot{U}_{P1} = -\frac{1}{C_{P1}R_{P1}}U_{P1} + \frac{1}{C_{P1}}I \quad (11)$$

$$\dot{U}_{P2} = -\frac{1}{C_{P2}R_{P2}}U_{P2} + \frac{1}{C_{P2}}I \quad (12)$$

The fourth model type, shown in Figure 3d, is a source-dependent ECM introduced in [90]. This model is very reliable and could improve the battery's ability to identify non-linear dynamic activity. A self-discharge model of the battery's OCV–SOC activity is considered by resistor  $R_d$ , and battery capacity is modeled by  $C_c$ . The voltage–current characteristics are still modeled as a second-order ECM to link the SOC to OCV, but a “voltage-dependent voltage source” is used in lieu of the source of voltage. The work presented in [86,89,90] introduced the complex mathematical voltage–current equations and the ECM, and the input is  $I_b$ , the state variables are  $V_{P1}$  and  $V_{P2}$ , and the output is  $U_L$ .

An EChM, developed based on chemical and electrodynamic thermodynamics, mass transfer, and various battery factors [12], is applied to evaluate the efficiency of the battery. Domenico et al. [86] suggested an estimated EChM by considering multiple parameters, for example, microscopic current density, substrate concentration, and electrolyte concentration. A model with four sub-models was proposed by Zou et al. [91] to capture the electrical, thermal, electrochemical, and aging dynamics using a set of partial differential equations. Since the SOC is one of the model's outcomes, this may be computed by computing the equation of the system directly. For various Li-ion chemistries, Bartlett et al. [92] introduced a reduced-order EChM estimating cyclable lithium loss and the SOC using dual non-linear observers.

Reference [93] focuses on the analysis of cyclic stresses linked to varying Li-ion concentration gradients. Utilizing a perfectly elastic-plastic model, the stress field induced by diffusion is adjusted within a hollow core structure. Additionally, critical values, dependent on factors like the outer and inner radii ratio, core radius, and shell thickness, are determined based on the perspective of strain energy release rate. Furthermore, a correlation is established between the critical outer and inner radii ratio and the state of charge, specifically when a hollow core reaches full lithiation. Lastly, a three-dimensional phase diagram is developed to illustrate the interplay between shell thickness, the core's outer radius, and the ratio of outer and inner radii. In accordance with the electrochemical-thermal coupled model described in Reference [94], a coupled three-dimensional battery thermal management system (BTMS) has been developed. This innovative system seamlessly integrates composite boards and heat pipes to optimize its thermal performance. The primary objective of this research is to evaluate the thermal characteristics of various BTMS configurations employing different combinations of boards and pipes. The outcomes of this study unequivocally demonstrate that the BTMS configuration incorporating both heat pipes and a composite board exhibits superior effectiveness in enhancing heat performance, compared to a BTMS configuration utilizing only a single composite board. In this study, as a means of elucidating the intricate interplay among electrochemical processes, thermal dynamics, and diffusion-induced mechanical stresses, the authors in Reference [95] introduce a coupled electrochemical–thermal–mechanical model tailored for spiral-wound lithium-ion batteries. This model harmoniously integrates principles governing mass con-

servation, charge conservation, energy conservation, and mechanical conservation, along with considerations of electrochemical kinetics. A meticulous exploration is undertaken, involving a range of temperature and lithium concentration parameters, to scrutinize their collective impact on reaction rates and the transport of  $\text{Li}^+$  ions within the battery. The results obtained from this model are meticulously validated through finite element simulations, revealing its robust suitability in accurately capturing both the electrochemical performance characteristics and thermal behaviors of the battery, even under conditions of constant discharge current. This reference [96] investigates the influence of irradiation temperature, dose, and diffusion-induced stress on the mechanical responses of cylindrical lithium-ion batteries (LIBs). A novel electrochemical-irradiated plasticity model is introduced to describe the behavior of electrodes within these LIBs, taking into account the effects of diffusion-induced stress. To ascertain the model's accuracy, a rigorous validation is conducted by comparing its numerical predictions with experimental data.

### 3.1.2. Adaptive Filter Algorithm

In the Kalman filter (KF) approach, the state-space form is used to solve a number of mathematical equations [83]. By comparing the computed input and output data using the KF approach, it is possible to establish the minimum mean square deviation of the true state [33]. Robust and fixed-lag smoothing is of paramount significance within the context of the Kalman filter, offering the dual benefits of computational burden reduction and mitigation of numerical instabilities. In reference [97], an innovative robust fixed-lag smoother is introduced, specifically tailored to situations where the actual model diverges from the nominal one. This approach is characterized by a minimax game, involving two key players: one is tasked with selecting the most challenging model from a predefined ambiguity set, while the other devises the optimal estimator based on this challenging model. Furthermore, the paper presents an efficient implementation of the robust fixed-lag smoother, strategically designed to minimize computational overhead and eliminate concerns related to numerical instabilities. But the KF cannot handle the non-linear characteristics of several battery kinds. For non-linear applications, this is why an extended Kalman filter (EKF) approach is commonly applied. To linearize the battery model, the EKF applies first-order Taylor series expansion and partial derivatives. Despite the batteries' highly non-linear thermal and electrochemical models, the EKF is utilized to approximate their properties, followed by the SOC [98,99]. In [100], an enhanced Thevenin battery model is used in conjunction with an adaptive extended Kalman filter (AEKF) to provide an accurate and robust SOC. This approach decreased SOC error from 3.16 to 1.06% and showed that the AEKF is superior to the EKF. The Taylor series expansion's first or second order terms are used in the EKF linearization approach for approximating a non-linear model [89]. The unscented Kalman filter (UKF) extracts the non-linear system statistical distribution features utilizing a sequence of sigma points to solve this problem instead of employing local linearization [101]. In addition to eliminating the requirement to build a Jacobian matrix, the UKF based on unscented transform estimates noise statistics more precisely than the EKF [102]. For UKF-based SOC calculation, through coulomb counting, He et al. [103] found voltage and the SOC. The UKF is applied to change the model factors automatically to reduce the error of the SOC induced as a result of changes in the environment and battery self-discharge. For SOC online calculation on the basis of an adaptive unscented Kalman filter (AUKF), Sun et al. [104] suggested a model of zero-state hysteresis that adaptively corrects measurement state and the noise covariances in the system. Moreover, it is easy to apply this strategy and needs less energy because of the easy zero-state hysteresis model system. In [105], an extreme learning machine (ELM) was applied to evaluate the AUKF-dependent SOC for a LIB, which needs less computing load to change the model factors based on experimental results. The sigma-point Kalman filter (SPKF), which uses a limited set of functions in terms of mean and covariance, is used to estimate states in the non-linear scheme and yields more accurate results than the EKF. The method selects sets of sigma points that are precisely close to the mean value and covariance

of the model being built. SOC estimation based on the SPKF is proposed in [106], where SOC estimation is performed by taking the connection between the SOC and OCV into account. In [107], three model-based methods, including the SPKF, EKF, and Luenberger observers, are used to compare SOC estimates for LiFePO<sub>4</sub> batteries. The findings of this experiment show that considering the impact on battery tracking precision and reliability, the SPKF increases the accuracy of the SOC estimate and provides consistency in numerical computations compared to measuring Jacobian matrices. However, it is a complex method and therefore requires heavy calculations [33]. The H $\infty$  filter is another method that takes into account time-varying battery factors and requires no knowledge of process noise requirements or noise measurement features [33]. To achieve the OCV–SOC relationship, Xiong et al. [108] introduced a time-saving approach by applying the H $\infty$  filter via some established current and voltage measurements. Yu et al. [109] used the H $\infty$  method to map the factors online in accordance with the operational conditions and used the UKF to calculate the SOC. An adaptive model-based SOC estimate is proposed in [110] that uses a recurrent neural network (RNN). With the support of the forgetting element, the RLS algorithm was applied to approximate the model parameters. This model compared the error, which was under 5%, between expected and actual capacity.

### 3.1.3. Learning Algorithm

Using objective criteria, the problem-solving method of fuzzy logic (FL) determines the precise values of the input data that are noisy, ambiguous, and uncertain. A fuzzy-rule-based system is utilized in [111] to figure out a KF's non-linear gain for SOC calculation. A merged fuzzy neural network (FNN) is presented in [112] for predicting the SOC of a LIB using a reduced-form genetic algorithm (RGA). To estimate the SOC, adaptive neuro-fuzzy inference systems (ANFISs) are more effective [113,114]. ANFISs can be implemented for cell characteristics modeling [115], for online correction of other SOC measurement processes to develop high accuracy [116], or for directly estimating the SOC [117]. An offline power system application model is presented in [115] for SOC measuring in LIBs. Here, the ANFIS battery model is learned offline on the basis of the manufacturer data on LIBs and improved to grow the cell's SOC and OCV within the learning range at any temperature. A regression technique is used to turn a lower-dimensional non-linear model into a linear higher-dimensional model using the kernel-function-based support vector machine (SVM) [33]. The SVR algorithm was applied in [118], for estimating a high-capacity LIB's SOC where independent factors, for example, current, voltage, and temperature, were necessary for determining the factors of the model during the discharging/charging condition. Having a 0.97 expected coefficient of determination, this model offered a good degree of SOC accuracy. Least-squares support vector machine (LS-SVM)-based SOC approximation was introduced in [119] that involved the relationship of temperature, current, and voltage for SOC estimation which indicates high accuracy, quickness, and noise-tolerant ability in predicting the SOC. The self-learning and adaptability of a neural network (NN) allow it to explain a complicated non-linear model. This method applies learned data for estimating the SOC from unknown battery internal structure and the initial SOC. For the creation of an NN network, three layers are used: a hidden layer or layers, an output layer, and an input layer, as depicted in Figure 4 [120–122]. The inputs of the NN network structure are discharge current, terminal voltage, and temperature, while the output is the SOC. Considering the impact of OCV hysteresis, Chen et al. [121] proposed an EKF-based model. After that, the NN and EKF were integrated for the SOC estimate. The combined model suggested offers the highest value in predicting precision, whose margin of error is less than 1%.

### 3.1.4. Non-Linear Observers

The non-linear observer (NLO) is applied with non-linear observation equations in a linear system. Xia et al. [123] recommended applying an RC equivalent circuit of the first order for the NLO-based SOC estimation of a LIB. Applying the ninth-order polynomial

and the state space equations, the SOC was estimated from OCV. Validation of this model was conducted by discharge testing. The findings revealed that, in terms of precision, convergence speed, and computational cost, the recommended approach is superior to the EKF and sliding mode observer (SMO). To account for the battery's non-linear dynamic features, Kim et al. [81] developed an SMO-based SOC estimation technique applying a simple RC circuit. The time of convergence might be controlled by using the suggested method even at high charge/discharge levels. Huanchun et al. [124] recommended an approach for SOC estimation depending on second-order SMO.

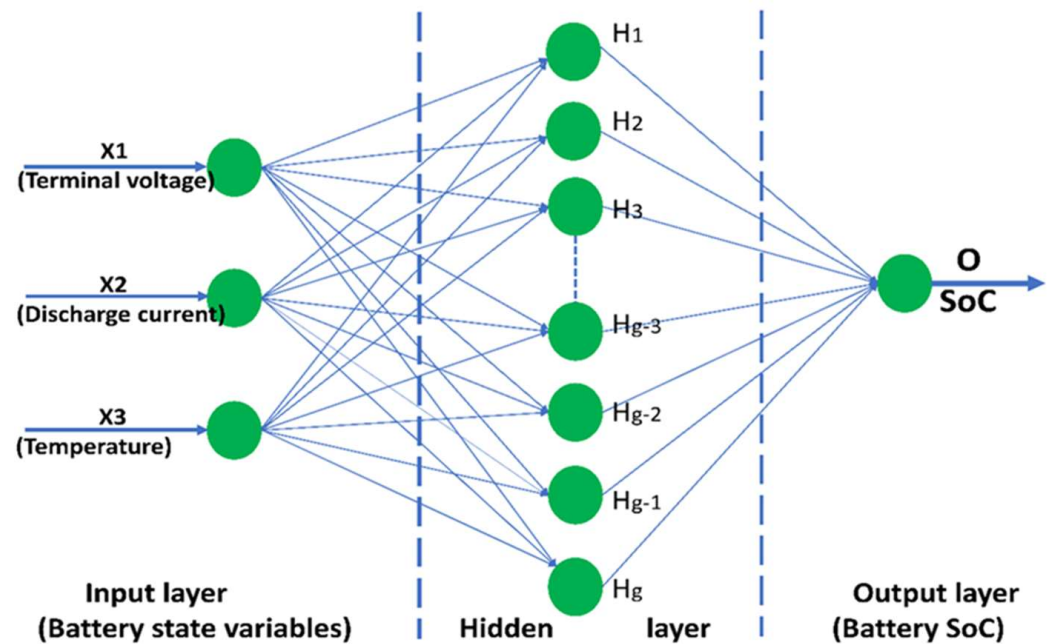


Figure 4. The entire structure of NN for SOC estimation.

### 3.1.5. Others

A statistical learning methodology was proposed called multivariate adaptive regression splines (MARS), in which optimum factors were determined by using the particle swarm optimization (PSO)-based SOC measuring technique [125]. The method has a drawback which is that at the beginning and end of the SOC cycle, the precision disperses. To compare a linear time-invariant (LTI) device's output to a random output, infrared (IR) is applied. Ranjbar et al. [126] used the method for online SOC calculation. The expected value calculated by IR is ideally matched to the actual SOC value. SOC prediction based on linear interpolation can be performed using the charging/discharging characteristics of the battery [33]. A scalable approach was created based on a derivation of gradient boosting called XGBoost "eXtreme gradient boosting" as in 2015 which is applied for measuring the SOC under complex working situations based on discharge test results, and the calculation has a 98.81% coefficient of determination. Liye et al. [127] recommended a bi-linear interpolation algorithm to apply a 3D look-up table to an approximate SOC. Initially, the steady-state charging and discharging current's linear interpolation was investigated. Then, by applying the current and voltage value, the bi-linear interpolation technique was created using a 3D SOC look-up table. This method ensures stability in execution. Table 2 [128,129] provides an overview of the evaluation results from several techniques.



**Table 2.** The outcomes of various methods for estimating SOC.

Approach	Computational Complexity	Evaluation Index	Estimation Precision	Refs.	
Coulomb counting	Hybrid pulse power characteristic test and model-based dynamic multi-parameter method	Estimation error	4%	[130]	
Open-circuit voltage	Non-linear estimation algorithm, logarithmic function, exponential function, linear function, and electrochemical processes	Estimation error	0.5%	[131]	
Impedance measurement	Function expressions and model	Absolute error	Less than 15%	[132]	
Kalman filtering	Pulse charging process, stochastic state-space model, and Riccati differential equations	Error	1.76%	[133]	
Extended Kalman filtering	Hardware-loop test and matrix operation, model	Mean square state error	3%	[134]	
Adaptive extended Kalman filter	Matrix operation, model	Root mean square error	Less than 2%	[135]	
Unscented Kalman filter	Linear averaging method, capacitance correction factor, resistance, correction factor, and model	Maximum error	4.12%	[101]	
Sigma-point Kalman filter	Non-linear function	Root mean square (RMS) error	0.49%	[136]	
Equivalent circuit model	Current time constant expression and logarithmic function	Estimation error	<2.5%	[137]	
Electrochemical model	Moving-window filter and transfer function	Root mean square (RMS) error	12%	[138]	
Artificial neural network (ANN)	A variant—long short-term memory (AST-LSTM) and matrix operation	Average root mean square error	2.16% (SOH), 2.02% (RUL)	[139]	
	Long short-term memory (LSTM), recurrent neural network (RNN), and matrix operation	Mean absolute error	N/A	[140]	
Fuzzy logic	Supervised and unsupervised learning techniques, Mamdani, and the first-order Sugeno approach	Maximum error	5%	[141]	
Recursive least squares (RLS)	Differential of the voltage, SOC difference, capacitance, and ohmic resistance	Estimation error	Less than 2.7%	[142]	
Relevance vector machine (RVM)	Matrix operation and RVM	Root mean square (RMS) error	<0.4%	[143]	
Support vector machine (SVM)	Matrix operation, SVM	Mean absolute error	0.0223 Ah	[144]	
Genetic algorithm	Online identification algorithm and coulomb counting method	Estimation error	Less than 1%	[145]	
H $\infty$ Filter	Matrix operation, model	Estimation error	2.49%	[146]	
Hybrid model	Model-based + Data-driven	Particle filter (PF), Brownian motion (BM), and matrix operation	Root mean square (RMS) error	Less than 4% (SOH)	[147]
	Direct measurement + Model-based method	Forgetting factor recursive least squares (FFRLS) and double polarization model	Error	3%	[148]

### 3.2. SOH Estimation

A battery cell’s current health relative to its ideal conditions is measured by its state of health (SOH) [149]. There is no one term that best describes the battery SOH. Battery SOH may be explained generally as follows [150]:

$$SOH(t) = SOH(t_0) + \int_{t=t_0}^t \delta_{func}(I, T, SOC, others) d\tau \tag{13}$$

where the original SOH battery is  $SOH(t_0)$ , and  $\delta_{func}$  is an aging rate feature that significantly depends on several factors, including the current, temperature, SOC, and a number of additional stressors, including over-potential and mechanical vibrations [150]. The SOH can be derived from capacity and internal resistance, as well as additional battery characteristics including power density, self-discharge intensity, and AC impedance [12]. A battery cell’s SOH decrease is often caused by the aging and deterioration of the battery, specifically, longevity issues. That means that the battery capacity would decrease with the usage or storage of the battery cells, and there would be more internal resistance [12]. The battery cells’ SOH gets worse as a result. This is why a precise assessment of the SOH is required, which may be performed using a multitude of methods.

Model-based approaches are one of the most widely utilized online methods for SOH prediction. One of them is empirical models (EMs), which are produced by fitting experimental data gathered under established experimental settings and utilized to connect deterioration variables to battery SOH. Battery cycle testing, where capacity fading is shown as a function of time or of the number of cycles, is used to suit the specific empirical equivalence [151–153]. Table 3 summarizes the fitting models that have been built based on the cycle testing and have shown to be efficient in SOH estimation [152]. When the batteries are exposed to similar operating circumstances to the modeling scenario, they often have high computational performance and may obtain satisfactory estimation precision [154]. However, modern EMs still have a lot of limitations when it comes to estimating battery SOH [154]. Comprehensive aging tests must be undertaken in order to produce an empirical SOH model. These procedures are frequently time-consuming and tedious. Furthermore, the developed model’s resistance to unknown operating circumstances is inadequate, and it lacks sufficient generality to other battery chemistries or even different quantities of the same chemistry [152].

**Table 3.** An overview of empirical models for estimating SOH.

Empirical Models	Estimation Factors	Estimation Precision	Model Formula	Refs.
Linear models	Capacity	R-square: 0.9778	$f(k, I) = \beta_1(k) + \beta_2(k) \cdot I + \varepsilon(k)$	[155]
	Capacity	root mean square (RMS) error: 0.67%	$c_k = \gamma - \beta k$	[156]
Exponential models	Capacity	R-square: 0.9844	$lnf_1(n, t) = (\eta_1 + \eta_2 n) \exp(\eta_3 T) + \varepsilon_1(n)$	[155]
Hybrid model	OCV and capacity	Relative error: less than 0.45%	$OCV(SOC, T) = \exp\left[\frac{E}{R} \left(\frac{1}{T_{ref}} - \frac{1}{T}\right)\right] \cdot \sum_{k=0}^m a_{k,ref} SOC^k$	[157]
	Capacity	Root mean square (RMS) error: 0.67	$c_k = 1 - \alpha[1 - \exp(-\lambda k)] - \beta k$	[156]

Electrochemical models (EChMs) and electrical equivalent circuit models (ECMs), both of which are primarily physical-based models, are two more model-based methods. The ECM is the simplest model that applies particular elements including a voltage, capacitor, and resistor source for describing the extremely dynamic behavior of LIBs [152]. ECM-based techniques consider the battery’s electrical properties, making it simple to implement and extract the deterioration feature [152]. Some adaptively filtering algorithms, such as the PF [158], EKF [159], and AEKF [160], are used to identify electrical variables including capacity and resistance for the battery SOH prediction based on established ECMs, such as the RC model [161] and fractional-order model (FOM) [162]. Another important method is the EChM. Depending on the chemical processes occurring inside the battery, the EChM [163] predicts the behavior of the battery. The EChM-based technique may more

accurately estimate the SOH by reflecting the complex electrochemical process, such as the creation of the SEI.

To get sensitive SOH-related properties, based on the differentiation of curves, differential analysis (DA) in the context of batteries incorporates electrical, thermal, or mechanical data obtained during galvanostatic charge or discharge. The IC/DV (incremental capacity/differential voltage) method of cell characterization is non-destructive. By dividing the modification of battery capacity by the modification of terminal voltage ( $dQ/dV$ ), incremental capacity (IC) is calculated over a sufficiently short time span, whereas by dividing the battery voltage by the capacity ( $dV/dQ$ ), DV is calculated, which may be applied for differentiating the aging procedures taking place in batteries. With fading battery capacity, the peak amplitudes drop [164], and the reported peak locations alter [165] in the IC/DV curve [152]. For a precise SOH computation, the partial  $dQ/dV$  information was additionally analyzed using gray relational analyses and the entropy weight technique, depending on the unambiguous peak properties in the voltage zones [166]. Additionally, a useful technique for calculating the SOH online is IC/DV analysis [165] which can be readily implemented in a BMS by monitoring only two parameters (voltage and discharge/charge capacity) and also is applicable for all types of Li-ion cells, regardless of battery chemistry, size, or design. This approach is only useful for determining the SOH of a battery at modest charge/discharge rates. The over-potential induced by the cell's impedance, which depends more on temperature than on age [154,167,168], offsets the peaks at high current rates. To provide a more precise measurement of the SOH, IC/DV is usually stimulated at a low current rate. In several practical applications, however, ensuring a low discharging current rate may not be feasible [169]. Furthermore, because of the evident impedance shift at high current rates, the peak is prone to being offset [168]. These restrictions have a significant impact on online SOH estimate accuracy. As a result, it is critical to use proper filtering and smoothing procedures to decrease measurement noise [167]. The first and most important step in SOH analysis is smoothing, and a multitude of filtering techniques may be used to achieve it, including the moving average [170], Gaussian filter [165], and Savitzky Golay filter [171,172]. In any practical application of IC/DV curves, temperature can induce considerable inaccuracies [154].

Furthermore, differential thermal voltammetry (DTV) may be used in SOH estimate complementary analysis. It uses temperature information and the idea of IC analysis to deduce the thermodynamic properties of the electrode material [152,172]. This approach takes into account temperature changes with  $dT/dV$  and adds further entropic characteristics to IC/DV methods [41] to obtain a more precise evaluation at high current rates [173]. The entropy characteristics that represent the fluctuation of peak amplitude and locations are utilized to signify the growth of LIB deterioration and impedance in the  $dT/dV$  curve [172]. Even though the DTV analysis is simple, swings in the ambient temperature can add a lot of noise, and the measurement temperature setting has a lot of influence, making it difficult to extract relevant data and analyze them further [41]. Furthermore, several mechanical characteristics are linked to cell SOH, including strain ( $\epsilon$ ) and stress [174], and load sensors positioned on the battery surface may be used to detect the SOH because the stress caused by electrode expansions is linearly connected to the SOH. A few research studies on the first derivative of strain to voltage ( $d\epsilon/dV$ ) [175] and capacity ( $d\epsilon/dQ$ ) [171] have served as the foundation for the SOH calculation, as well as the second derivative of strain to capacity ( $d\epsilon^2/dQ^2$ ) [176]. The negative electrode's phase changes are identified using the  $d\epsilon/dQ$  curves. At some voltages, phase transitions are responsible for the rise in strain seen in the  $d\epsilon/dV$  graphs as a function of voltage. Phase transitions in electrode materials were discovered using the  $d\epsilon^2/dQ^2$  curves, which allowed for higher current rates than the DV analysis [41]. The phase transitions in both negative and positive electrode materials may be seen in these curves, which are equivalent to IC/DV analysis. Based on the expansion identification, the differential mechanical parameter (DMP) analysis can be utilized to estimate the SOH at low or high current rates. In reality, a battery pack's space is constrained by the number of batteries it can hold [152].

Instead of applying complex battery concepts, data-driven techniques calculate the SOH based on the physical relationship between battery health and other feature variables using optimization algorithms, machine learning, empirical fitting, and sample entropy. The SOH estimate using data-driven approaches cannot accurately capture the battery's physical characteristics of a battery. As a result, data-driven procedures are frequently integrated with the above-mentioned experimental methods. Specialized battery tests are first performed in the corporate setting to identify all SOH-influencing elements, and then using data-driven approaches, a battery SOH model is developed by connecting these impacting elements with the battery SOH. On the other hand, the quality and quantity of test data have a substantial impact on these approaches' performance, and the resulting model is often subject to high computational intensity [41,154]. In terms of significant benefits and downsides, SOH estimation approaches are mentioned in Table 4 [152,154].

**Table 4.** Methodologies for SOH estimate in terms of important advantages and disadvantages.

Method		Benefits	Drawback
Model-based method	Physics-based model	High accuracy, clear meanings	Heavy computational load, difficult model parameterization
	Empirically based model	Simple structure, easy implementation	Poor robustness, relatively low accuracy
Differential analysis method		Simple structure, easy implementation	Unguaranteed precise online SOH estimation under different working conditions
Data-driven method		No requirement for the knowledge of underlying mechanisms	Sensitive to quality and quantity of data. Potential over-fitting problems

### 3.3. Others

How the battery output complies with the actual standards is explained using the state of function (SOF) [12] when the battery is used. Some of the factors include temperature, the battery's terminal voltage, the state of power (SOP), the SOH, the SOC, and, more influential, the SOF of the battery. The SOF of a single cell may easily be obtained if the SOH and SOC of the cell are known. The SOF could be represented as the logical variable yes/no [177]. If the value of both the SOC and SOH is low, then the SOF value would be 0. The SOF would be 1, for both the high value of the SOH and SOC. If the SOC and SOH values are different, then either 1 or 0 [178] can be the SOF. If the SOF is equal to 1, the battery could fulfill the specifications, and if the SOF is equal to 0, then it cannot fulfill the specifications. But practically, because of the battery uniformity issues, the battery module's SOF is more significant and challenging to calculate. It would be more desirable, however, to describe the SOF as the following equation [12,179].

$$P(t) = P_{max}.SOC(t).SOH(t) \quad (14)$$

$$SOF = \frac{P(t) - P_{demands}}{P_{max} - P_{demands}} \quad (15)$$

where  $P$  implies the instantaneous power the battery might provide, the  $P_{demands}$  implies the power specifications, and the  $P_{max}$  implies the overall possible battery power supply. The SOC and SOH's rates of change are different as the temperature increases, and it can be concluded that the SOC, SOH, and battery operating temperature are all directly connected to the SOF [180].

It is difficult to accurately assess the battery's internal temperature without causing any damage because battery packs are complicated electrochemical systems [31]. Furthermore, battery recyclability, reliability, power, and energy performance are all influenced by operat-

ing temperatures [181]. As a result, an accurate state of temperature (SOT) estimate becomes essential and critical. The specific meaning of the SOT is still to be determined [182]. The battery temperature distribution may be estimated online using a variety of observers, along with simple thermal models or empirical impedance models, and based on observable temperature (such as the ambient temperature and surface temperature) [154]. Li et al. [183] studied the thermal properties of overcharging at 30 and 60 degrees Celsius using an impedance-based electro-thermal model. To detect overcharging, an electrothermal model was proposed, which decreased estimation errors considerably at 0.9 °C. A monotonic relationship between battery internal temperature and impedance was established by Zhang et al. [184], based on a simple thermoelectric model to predict the internal temperature. Battery internal temperature and impedance phase change were linked at 10 Hz, according to Zhu et al. [185]. However, because of the intricate interconnections of nearby cells and heat conductions, a battery module or pack's SOT calculation is still lacking [154]. Furthermore, additional research and inquiries into how to construct a better thermal model that achieves the necessary balance between effectiveness and computing effectiveness are required [154].

The amount of power a battery is capable of providing to or drawing from a device across a time horizon is known as the state of power (SOP) [186]. It is a measure of the battery's instantaneous power output capability and is affected by various factors such as the battery's internal resistance, temperature, and aging. This may be regarded as a function of threshold voltage and current, with different functional restrictions to be explicitly examined and followed [154]. The reference values of the SOP are often derived under simulation circumstances using a high-fidelity battery model that takes into account numerous limitations [187]. The SOP may be determined using characteristic map (CM)-based approaches and model-based methods. Model-based approaches, for example, the least-squares-based method [187], particle filter [188], the Kalman filter [189], and others, have been effectively used to provide appropriate SOP estimates [154]. Model-based methods are simple and extensive. However, the use of this estimation method is still scarce in the literature. The past and present information on batteries, on the other hand, is hard to consider using CM-based methods, which are straightforward to apply. The precision of the SOP estimate would be substantially compromised since battery power is very dependent on operational conditions [154].

### *3.4. Summary of Comparison of Other Review Papers*

Unlike many other scholarly reviews that primarily focus on specific aspects such as the state of charge (SOC), state of health (SOH), or battery performance measurement, this paper offers a comprehensive examination that spans a wide range of topics. This holistic approach aims to equip readers with a deep and relevant understanding. Specifically, the paper delves into the mechanisms of battery aging, their origins, techniques for estimating battery state, and various interconnected subjects. It is important to acknowledge that there is no universally applicable method or approach that guarantees effectiveness in all scenarios. Designers must meticulously evaluate the unique requirements and constraints of each application to select the most suitable approach. The insights presented in this paper constitute a valuable resource for both researchers and practitioners engaged in battery management and electric vehicles. Looking ahead, it is imperative to explore aging processes and degradation models at the individual cell level, particularly in terms of how different factors influence battery lifespan, power output, and energy density. Understanding these aging processes and degradation models is also of great significance at the battery system level, as it aids in assessing battery health, optimizing current operational conditions, and forecasting future performance. In this context, Table 5 provides a visual representation of the relevant data.



**Table 5.** A comparative analysis of review papers on battery aging and state estimation.

Reference	Review of Battery Aging	Review of State Estimation		
		State of Charge (SOC)	State of Health (SOH)	Others
[4]	X	X	Review on SOH forecast	X
[186]	X	Brief SOC discussion	X	Review on state of power (SOP) prediction
[182]	X	Review on SOC prediction	Review on SOH prediction	Review on state of function (SOF), state of temperature (SOT) prediction
[152]	X	Review on SOC estimation	Review on SOH prediction	X
[150]	Review of battery degradation	X	X	X
[128]	X	X	Review on SOH estimation	X
[89]	X	Review on SOC estimation	X	X
[30]	Brief discussion on battery degradation	X	Review on SOH estimation	X
[26]	Review on battery aging degradation	X	X	X
[23]	Review on battery aging degradation	X	X	X
[190]	X	Review on SOC estimation	Review on SOH prediction	Review on SOP prediction
[191]	X	Review on SOC prediction	Review on SOH prediction	X
[192]	X	Review on SOC estimation	Review on SOH prediction	Review on SOP prediction
This paper	Review on battery aging degradation	Review on SOC estimation	Review on SOH prediction	Review on state of function (SOF), state of temperature (SOT) prediction, SOP

## 4. Future Trends

### 4.1. Challenges

Battery state estimation is the process of estimating the state of a battery, based on available sensor measurements and other relevant information. The accurate estimation of battery states is crucial in various applications, such as electric vehicles, renewable energy systems, and portable electronics, as it ensures the safe and efficient operation of the battery system. However, there are several challenges associated with the state estimation of batteries as mentioned below:

*Non-linear behavior of the battery:* LIBs exhibit non-linear behavior due to the complex electrochemical processes involved in the charge and discharge cycles. Accurate SOC estimation requires models that capture this non-linearity, but such models can be difficult to develop and computationally expensive to implement in real-time systems.

*Thermal effects:* Temperature variations within the battery pack can affect the accuracy of SOC estimation. High temperatures accelerate the battery's aging process, while low temperatures reduce the battery's capacity, making it challenging to accurately estimate the SOC.

*Battery degradation:* LIBs degrade over time, reducing their capacity and altering their behavior. This degradation makes it difficult to accurately estimate the SOC, as the battery's characteristics change over time.

*Model uncertainty:* The accuracy of SOC estimation relies heavily on the quality of the battery model used. Model uncertainty, arising from errors in the battery model or inaccurate model parameters, can significantly affect the accuracy of SOC estimation.

*Measurement noise:* Noise in the battery's current and voltage measurements can adversely affect the accuracy of SOC estimation. Accurate measurement of these parameters is essential for precise SOC estimation.

*Battery aging:* The aging of a LIB affects its internal resistance and its capacity, leading to changes in the battery's behavior. These changes can make it challenging to accurately estimate the SOC of an aged battery.

*Voltage hysteresis:* LIBs exhibit hysteresis in their voltage response during charging and discharging cycles, which can result in inaccuracies in SOC estimation. Accurate modeling and compensation for voltage hysteresis are crucial for precise SOC estimation.

*Limited data availability:* In some cases, limited data may be available for developing battery models, which can make accurate SOC estimation challenging. This problem can be overcome by using data-driven approaches, such as machine learning, to develop accurate models of battery behavior.

Overall, accurate SOC estimation for LIBs remains a challenging problem due to the complexity of the battery behavior and the many factors that can affect it. Nonetheless, recent research has made significant progress in addressing these challenges and developing new techniques for accurate SOC estimation which are mentioned below:

*Deep-learning-based SOC estimation:* Deep learning algorithms, such as neural networks, have shown promising results in accurately estimating the SOC of LIBs. These algorithms can learn complex relationships between input data, such as battery voltage and current, and the SOC, without the need for complex battery models.

*Extended Kalman filter with adaptive gain:* The extended Kalman filter (EKF) is a popular method for SOC estimation, but its performance can be sensitive to model uncertainties and measurement noise. Recent research has proposed an adaptive gain EKF, which adjusts the EKF's gain based on the quality of the input data, to improve the accuracy of SOC estimation.

*Hybrid models for aging-aware SOC estimation:* Battery aging affects the accuracy of SOC estimation, and recent research has proposed hybrid models that combine physics-based models with data-driven models to account for aging effects. These models can accurately estimate the SOC of aged batteries, improving battery management and prolonging battery life.

*Data-driven SOC estimation using big data analytics:* Recent research has proposed data-driven approaches for SOC estimation, which leverage big data analytics to develop accurate models of battery behavior. These approaches can improve the accuracy of SOC estimation, even when limited data are available for developing battery models.

However, in the context of estimating the battery condition, thermal runaway is, nonetheless, a crucial factor, particularly for LIBs. When a battery experiences thermal runaway, its temperature rises uncontrollably, frequently resulting in catastrophic failure, fire, or explosion. Particularly in applications where batteries may be subjected to harsh circumstances or abuse, accurate estimation and prediction of thermal runaway are essential for maintaining the safety of battery systems. Here are some of the challenges associated with battery state estimation in the presence of the thermal runaway problem:

*Early Detection:* The early detection of thermal runaway is one of the main challenges. It is essential to foresee when a battery may reach a thermal runaway scenario in order to take preventative action. The requisite thermal models and data may not be included in conventional state estimate methods in order to effectively predict impending thermal runaway.

*Thermal Model Complexity:* The necessity for extremely intricate thermal models is brought on by thermal runaway. These models must take into consideration a number of things, including the complex processes involved in heat generation and dissipation, thermal feedback mechanisms, and the effects of outside variables like ambient temperature. Such models can be difficult and computationally intensive to develop and apply.

*Data Availability:* It is necessary to have access to reliable temperature data from the battery pack in order to estimate the battery's state accurately, especially when it comes

to thermal runaway. It is crucial to check that temperature sensors are set and calibrated properly. It may not always be possible to collect precise temperature data, which makes estimates more difficult.

*Real-Time Processing:* The computing requirements of precisely calculating the battery condition in the context of thermal runaway can be a substantial problem for applications where real-time monitoring and control are essential. Accuracy and the need for real-time processing must be delicately balanced.

*Non-linearity and Uncertainty:* The non-linearity and unpredictability that are already present in battery performance are made worse by thermal runaway. Accurate estimation becomes increasingly more difficult as a battery approaches thermal runaway because of behavior that may differ significantly from nominal settings.

*Safety Implications:* Dealing with thermal runaway is risky since it can result in explosions and flames, both of which pose serious safety risks. Serious repercussions may result from any errors or lags in state estimates. The utmost level of accuracy and dependability in estimate methods must therefore be guaranteed.

*Integration with Safety Systems:* Safety features are usually included in battery management systems (BMSs) to handle the potential of thermal runaway. A thorough safety strategy must coordinate the state estimation process with various safety systems, such as thermal cutoff switches and cooling controllers.

*Aging Effects:* The state estimate is further complicated by the fact that thermal runaway can be affected by battery aging. The estimating procedure must take into account modifications in a battery's thermal behavior brought on by aging.

*Fault Tolerance:* Given the critical nature of thermal runaway, fault tolerance should be considered while designing state estimation algorithms. In the event of algorithmic failures, redundancy and fail-safe techniques may be required to ensure continuing operation.

*Validation and Testing:* Due to the possible safety issues involved, it can be difficult to verify the precision and dependability of state estimate methods under thermal runaway situations. It is crucial to create precision testing processes and validation protocols.

Overall, recent research has proposed a range of innovative approaches to improve the accuracy of SOC estimation for LIBs.

#### 4.2. Future Research Direction

The field of state estimation for LIBs is rapidly evolving, and there are several future trends that are expected to have a significant impact on the field. Here are some of the trends that are likely to shape the future of SOC estimation for LIBs:

*Integration of multiple sensing modalities:* The integration of multiple sensing modalities, such as temperature, pressure, and humidity, with traditional voltage and current measurements, can provide more comprehensive information about the battery state, improving the accuracy of SOC estimation.

*Machine-learning-based approaches:* Machine learning algorithms, such as deep neural networks, have shown promising results in accurately estimating the SOC of LIBs. Future research is expected to further explore and optimize these approaches to achieve even higher accuracy and reliability.

*Model-based deep reinforcement learning:* Model-based deep reinforcement learning (DRL) combines the advantages of physics-based battery models with the power of deep learning algorithms. Future research is expected to explore the potential of DRL for SOC estimation, which can provide more accurate and robust estimates of the battery state.

*Hybrid modeling approaches:* Hybrid modeling approaches, which combine physics-based models with data-driven models, can account for the complex and dynamic behavior of LIBs. Future research is expected to explore and optimize these approaches for more accurate and reliable SOC estimation.

*Advanced data analytics:* The use of advanced data analytics techniques, such as big data analytics and cloud computing, can improve the accuracy and scalability of SOC

estimation for LIBs. Future research is expected to leverage these techniques to develop more accurate and efficient SOC estimation algorithms.

Overall, the future of SOC estimation for LIBs is expected to be characterized by the integration of multiple sensing modalities, the use of advanced machine learning algorithms, and the development of hybrid modeling approaches that can account for the complex and dynamic behavior of LIBs.

## 5. Conclusions

In conclusion, the battery management system (BMS) plays a pivotal role in ensuring the safe operation and optimal performance of electric vehicle battery packs. While numerous studies and technologies have been developed to enhance battery pack monitoring and control, they encompass a wide spectrum of approaches, ranging from basic monitoring techniques to advanced control systems. Nevertheless, a central challenge in developing an effective BMS lies in identifying and mitigating the diverse aging and degradation processes that can impact battery performance and longevity. This endeavor demands a deep understanding of the intricate mechanisms at play, as well as the ability to accurately measure critical metrics. A multitude of SOC measurement methods have been proposed, each with its distinct advantages and drawbacks. Conventional methods like open-circuit voltage (OCV), coulomb counting, and internal resistance testing are relatively straightforward but may lack the precision offered by more advanced techniques such as adaptive filter algorithms or non-linear observers. However, these advanced methods can be computationally intensive and may necessitate significant offline learning phases, rendering them less suitable for real-time applications in electric vehicles. Hence, the judicious selection of an appropriate method, contingent upon factors like accuracy, computational requirements, and real-time feasibility, is of paramount importance. In this context, this paper has furnished a comprehensive review of the myriad methods and technologies available for battery monitoring and management, elucidating their respective strengths and limitations. Furthermore, it has underscored other vital characteristics of battery packs that should inform the development of effective diagnostic parameters for estimating battery behavior. It is crucial to acknowledge that no single method or approach can offer universal effectiveness across all scenarios. Designers must meticulously consider the specific requirements and constraints of each application to select the most suitable method. The insights presented in this paper serve as a valuable resource for researchers and practitioners working in the realm of battery management and electric vehicles. Moving forward, investigating battery aging processes and deterioration models at the cell level, particularly in terms of how essential factors impact battery life, power, and energy density, is imperative. The understanding of aging processes and deterioration models also holds significant importance at the battery system level, aiding in estimating battery health, optimizing current operational conditions, and forecasting future performance.

The field of state estimation for lithium-ion batteries (LIBs) is undergoing rapid evolution, with several compelling trends poised to shape its future. These include the integration of multiple sensing modalities, the ongoing exploration and optimization of machine-learning-based approaches, the potential offered by model-based deep reinforcement learning (DRL) for state estimation, the refinement of hybrid modeling approaches capable of addressing the dynamic complexities of LIBs, and the leverage of advanced data analytics techniques like big data analytics and cloud computing. Collectively, these trends are anticipated to define the future landscape of SOC estimation for LIBs, enhancing accuracy and efficiency in understanding and managing the complex and dynamic behavior of these energy storage systems.

**Author Contributions:** All authors had an equal contribution in preparing and finalizing the manuscript. Conceptualization: P.K.R., M.S., T.S. and A.F.; methodology, P.K.R., M.S., T.S. and A.F.; validation: A.F., S.S., M.A. and J.H.; formal analysis: P.K.R., M.S., T.S., A.F., S.S., M.A. and J.H.; investigation: P.K.R., M.S., T.S. and A.F.; data curation: P.K.R., M.S., T.S. and A.F.; writing—original draft preparation: P.K.R., M.S., T.S., A.F., S.S., M.A. and J.H.; writing—review and editing: A.F.,

S.S., M.A. and J.H.; supervision: A.F., S.S., M.A. and J.H. All authors have read and agreed to the published version of the manuscript.

**Funding:** This research received no external funding.

**Institutional Review Board Statement:** Not applicable.

**Informed Consent Statement:** Not applicable.

**Data Availability Statement:** Not applicable.

**Conflicts of Interest:** The authors declare no conflict of interest.

## References

1. Sun, C.; Negro, E.; Vezzù, K.; Pagot, G.; Cavinato, G.; Nale, A.; Bang, Y.H.; Di Noto, V. Hybrid inorganic-organic proton-conducting membranes based on SPEEK doped with WO<sub>3</sub> nanoparticles for application in vanadium redox flow batteries. *Electrochim. Acta* **2019**, *309*, 311–325. [[CrossRef](#)]
2. Brandt, K. Historical development of secondary lithium batteries. *Solid State Ionics* **1994**, *69*, 173–183. [[CrossRef](#)]
3. Yoshino, A. The Birth of the Lithium-Ion Battery. *Angew. Chem. Int. Ed.* **2012**, *51*, 5798–5800. [[CrossRef](#)]
4. von Bülow, F.; Meisen, T. A review on methods for state of health forecasting of lithium-ion batteries applicable in real-world operational conditions. *J. Energy Storage* **2023**, *57*, 105978. [[CrossRef](#)]
5. Spanos, C.; Turney, D.E.; Fthenakis, V. Life-cycle analysis of flow-assisted nickel zinc-, manganese dioxide-, and valve-regulated lead-acid batteries designed for demand-charge reduction. *Renew. Sustain. Energy Rev.* **2015**, *43*, 478–494. [[CrossRef](#)]
6. Hu, X.; Zou, C.; Zhang, C.; Li, Y. Technological Developments in Batteries: A Survey of Principal Roles, Types, and Management Needs. *IEEE Power Energy Mag.* **2017**, *15*, 20–31. [[CrossRef](#)]
7. Wang, Q.; Jiang, B.; Li, B.; Yan, Y. A critical review of thermal management models and solutions of lithium-ion batteries for the development of pure electric vehicles. *Renew. Sustain. Energy Rev.* **2016**, *64*, 106–128. [[CrossRef](#)]
8. Xing, Y.; Ma, E.W.M.; Tsui, K.L.; Pecht, M. Battery management systems in electric and hybrid vehicles. *Energies* **2011**, *4*, 1840–1857. [[CrossRef](#)]
9. Song, S.; Zhang, X.; An, Y.; Hu, T.; Sun, C.; Wang, L.; Li, C.; Zhang, X.; Wang, K.; Xu, Z.J.; et al. Floating aging mechanism of lithium-ion capacitors: Impedance model and post-mortem analysis. *J. Power Sources* **2023**, *557*, 232597. [[CrossRef](#)]
10. Li, J.; Wang, S.; Fernandez, C.; Wang, N.; Xie, H. The battery management system construction method study for the power lithium-ion battery pack. In Proceedings of the 2017 2nd International Conference on Robotics and Automation Engineering, ICRAE 2017, Shanghai, China, 29–31 December 2017; Institute of Electrical and Electronics Engineers Inc.: Piscataway, NJ, USA, 2018; pp. 285–289. [[CrossRef](#)]
11. Zhang, M.; Liu, Y.; Li, D.; Cui, X.; Wang, L.; Li, L.; Wang, K. Electrochemical Impedance Spectroscopy: A New Chapter in the Fast and Accurate Estimation of the State of Health for Lithium-Ion Batteries. *Energies* **2023**, *16*, 1599. [[CrossRef](#)]
12. Lu, L.; Han, X.; Li, J.; Hua, J.; Ouyang, M. A review on the key issues for lithium-ion battery management in electric vehicles. *J. Power Sources* **2013**, *226*, 272–288. [[CrossRef](#)]
13. Shen, W.; Vo, T.T.; Kapoor, A. Charging algorithms of lithium-ion batteries: An overview. In Proceedings of the 2012 7th IEEE Conference on Industrial Electronics and Applications, ICIEA 2012, Singapore, 18–20 July 2012; pp. 1567–1572. [[CrossRef](#)]
14. Sun, Q. Electric vehicles: The breakthrough of ‘core’ is the key—Talking about three bottlenecks in the development of the Li-ion battery. *Adv. Mater. Ind.* **2010**, *12*, 62–63.
15. Zou, C.; Hu, X.; Wei, Z.; Tang, X. Electrothermal dynamics-conscious lithium-ion battery cell-level charging management via state-monitored predictive control. *Energy* **2017**, *141*, 250–259. [[CrossRef](#)]
16. Liu, K.; Li, K.; Yang, Z.; Zhang, C.; Deng, J. An advanced Lithium-ion battery optimal charging strategy based on a coupled thermoelectric model. *Electrochim. Acta* **2017**, *225*, 330–344. [[CrossRef](#)]
17. Shahriari, M.; Farrokhi, M. Online state-of-health estimation of VRLA batteries using state of charge. *IEEE Trans. Ind. Electron.* **2013**, *60*, 191–202. [[CrossRef](#)]
18. Lin, H.-T.; Liang, T.-J.; Chen, S.-M. Estimation of battery state of health using probabilistic neural network. *IEEE Trans. Ind. Inform.* **2013**, *9*, 679–685. [[CrossRef](#)]
19. Xiong, R.; Li, L.; Tian, J. Towards a smarter battery management system: A critical review on battery state of health monitoring methods. *J. Power Sources* **2018**, *405*, 18–29. [[CrossRef](#)]
20. Song, J.; Wang, Y.; Wan, C. Review of gel-type polymer electrolytes for lithium-ion batteries. *J. Power Sources* **1999**, *77*, 183–197. [[CrossRef](#)]
21. Sun, F.; Xiong, R. A novel dual-scale cell state-of-charge estimation approach for series-connected battery pack used in electric vehicles. *J. Power Sources* **2015**, *274*, 582–594. [[CrossRef](#)]
22. Vetter, J.; Novák, P.; Wagner, M.R.; Veit, C.; Möller, K.-C.; Besenhard, J.O.; Winter, M.; Wohlfahrt-Mehrens, M.; Vogler, C.; Hammouche, A. Ageing mechanisms in lithium-ion batteries. *J. Power Sources* **2005**, *147*, 269–281. [[CrossRef](#)]
23. Han, X.; Lu, L.; Zheng, Y.; Feng, X.; Li, Z.; Li, J.; Ouyang, M. A review on the key issues of the lithium ion battery degradation among the whole life cycle. *eTransportation* **2019**, *1*, 100005. [[CrossRef](#)]



24. Li, Z.; Huang, J.; Liaw, B.Y.; Metzler, V.; Zhang, J. A review of lithium deposition in lithium-ion and lithium metal secondary batteries. *J. Power Sources* **2014**, *254*, 168–182. [[CrossRef](#)]
25. Santhanagopalan, S.; Guo, Q.; Ramadass, P.; White, R.E. Review of models for predicting the cycling performance of lithium ion batteries. *J. Power Sources* **2006**, *156*, 620–628. [[CrossRef](#)]
26. Wang, A.; Kadam, S.; Li, H.; Shi, S.; Qi, Y. Review on modeling of the anode solid electrolyte interphase (SEI) for lithium-ion batteries. *NPJ Comput. Mater.* **2018**, *4*, 15. [[CrossRef](#)]
27. Barré, A.; Deguilhem, B.; Grolleau, S.; Gérard, M.; Suard, F.; Riu, D. A review on lithium-ion battery ageing mechanisms and estimations for automotive applications. *J. Power Sources* **2013**, *241*, 680–689. [[CrossRef](#)]
28. Xu, J.; Sun, C.; Ni, Y.; Lyu, C.; Wu, C.; Zhang, H.; Yang, Q.; Feng, F. Fast Identification of Micro-Health Parameters for Retired Batteries Based on a Simplified P2D Model by Using Padé Approximation. *Batteries* **2023**, *9*, 64. [[CrossRef](#)]
29. Farmann, A.; Waag, W.; Marongiu, A.; Sauer, D.U. Critical review of on-board capacity estimation techniques for lithium-ion batteries in electric and hybrid electric vehicles. *J. Power Sources* **2015**, *281*, 114–130. [[CrossRef](#)]
30. Berecibar, M.; Gandiaga, I.; Villarreal, I.; Omar, N.; Van Mierlo, J.; Van den Bossche, P. Critical review of state of health estimation methods of Li-ion batteries for real applications. *Renew. Sustain. Energy Rev.* **2016**, *56*, 572–587. [[CrossRef](#)]
31. Waag, W.; Fleischer, C.; Sauer, D.U. Critical review of the methods for monitoring of lithium-ion batteries in electric and hybrid vehicles. *J. Power Sources* **2014**, *258*, 321–339. [[CrossRef](#)]
32. Zhang, R.; Li, X.; Sun, C.; Yang, S.; Tian, Y.; Tian, J. State of Charge and Temperature Joint Estimation Based on Ultrasonic Reflection Waves for Lithium-Ion Battery Applications. *Batteries* **2023**, *9*, 335. [[CrossRef](#)]
33. Hannan, M.A.; Lipu, M.S.H.; Hussain, A.; Mohamed, A. A review of lithium-ion battery state of charge estimation and management system in electric vehicle applications: Challenges and recommendations. *Renew. Sustain. Energy Rev.* **2017**, *78*, 834–854. [[CrossRef](#)]
34. Dubarry, M.; Baure, G. Perspective on Commercial Li-ion Battery Testing, Best Practices for Simple and Effective Protocols. *Electronics* **2020**, *9*, 152. [[CrossRef](#)]
35. Shu, X.; Shen, S.; Shen, J.; Zhang, Y.; Li, G.; Chen, Z.; Liu, Y. State of health prediction of lithium-ion batteries based on machine learning: Advances and perspectives. *iScience* **2021**, *24*, 103265. [[CrossRef](#)]
36. Yao, L.; Xu, S.; Tang, A.; Zhou, F.; Hou, J.; Xiao, Y.; Fu, Z. A Review of Lithium-Ion Battery State of Health Estimation and Prediction Methods. *World Electr. Veh. J.* **2021**, *12*, 113. [[CrossRef](#)]
37. Wenzl, H.; Baring-Gould, I.; Kaiser, R.; Liaw, B.Y.; Lundsager, P.; Manwell, J.; Ruddell, A.; Svoboda, V. Life prediction of batteries for selecting the technically most suitable and cost effective battery. *J. Power Sources* **2005**, *144*, 373–384. [[CrossRef](#)]
38. Edge, J.S.; O’kane, S.; Prosser, R.; Kirkaldy, N.D.; Patel, A.N.; Hales, A.; Ghosh, A.; Ai, W.; Chen, J.; Yang, J.; et al. Lithium ion battery degradation: What you need to know. *Phys. Chem. Chem. Phys.* **2021**, *23*, 8200–8221. [[CrossRef](#)] [[PubMed](#)]
39. Birkl, C.R.; Roberts, M.R.; McTurk, E.; Bruce, P.G.; Howey, D.A. Degradation diagnostics for lithium ion cells. *J. Power Sources* **2017**, *341*, 373–386. [[CrossRef](#)]
40. Arora, P.; White, R.E.; Doyle, M. Capacity Fade Mechanisms and Side Reactions in Lithium-Ion Batteries. *J. Electrochem. Soc.* **1998**, *145*, 3647–3667. [[CrossRef](#)]
41. Li, Y.; Liu, K.; Foley, A.M.; Zülke, A.; Berecibar, M.; Nanini-Maury, E.; Van Mierlo, J.; Hoster, H.E. Data-driven health estimation and lifetime prediction of lithium-ion batteries: A review. *Renew. Sustain. Energy Rev.* **2019**, *113*, 109254. [[CrossRef](#)]
42. An, S.J.; Li, J.; Daniel, C.; Mohanty, D.; Nagpure, S.; Wood, D.L. The state of understanding of the lithium-ion-battery graphite solid electrolyte interphase (SEI) and its relationship to formation cycling. *Carbon* **2016**, *105*, 52–76. [[CrossRef](#)]
43. Zhang, S.; Ding, M.S.; Xu, K.; Allen, J.; Jow, T.R. Understanding solid electrolyte interface film formation on graphite electrodes. *Electrochem. Solid-State Lett.* **2001**, *4*, A206–A208. [[CrossRef](#)]
44. Ngo, D.-T.; Scipioni, R.; Simonsen, S.B.; Jørgensen, P.S.; Jensen, S.H. A TEM study of morphological and structural degradation phenomena in LiFePO<sub>4</sub>-CB cathodes. *Int. J. Energy Res.* **2016**, *40*, 2022–2032. [[CrossRef](#)]
45. Yang, X.-G.; Ge, S.; Liu, T.; Leng, Y.; Wang, C.-Y. A look into the voltage plateau signal for detection and quantification of lithium plating in lithium-ion cells. *J. Power Sources* **2018**, *395*, 251–261. [[CrossRef](#)]
46. Dubarry, M.; Beck, D. Big data training data for artificial intelligence-based Li-ion diagnosis and prognosis. *J. Power Sources* **2020**, *479*, 228806. [[CrossRef](#)]
47. Liu, X.M.; Arnold, C.B. Effects of Current Density on Defect-Induced Capacity Fade through Localized Plating in Lithium-Ion Batteries. *J. Electrochem. Soc.* **2020**, *167*, 130519. [[CrossRef](#)]
48. Bach, T.C.; Schuster, S.F.; Fleder, E.; Müller, J.; Brand, M.J.; Lorrman, H.; Jossen, A.; SEXTL, G. Nonlinear aging of cylindrical lithium-ion cells linked to heterogeneous compression. *J. Energy Storage* **2016**, *5*, 212–223. [[CrossRef](#)]
49. Yang, X.-G.; Leng, Y.; Zhang, G.; Ge, S.; Wang, C.-Y. Modeling of lithium plating induced aging of lithium-ion batteries: Transition from linear to nonlinear aging. *J. Power Sources* **2017**, *360*, 28–40. [[CrossRef](#)]
50. Campbell, I.D.; Marzook, M.; Marinescu, M.; Offer, G.J. How Observable Is Lithium Plating? Differential Voltage Analysis to Identify and Quantify Lithium Plating Following Fast Charging of Cold Lithium-Ion Batteries. *J. Electrochem. Soc.* **2019**, *166*, A725–A739. [[CrossRef](#)]
51. Zhao, X.; Yin, Y.; Hu, Y.; Choe, S.-Y. Electrochemical-thermal modeling of lithium plating/stripping of Li(Ni<sub>0.6</sub>Mn<sub>0.2</sub>Co<sub>0.2</sub>)O<sub>2</sub>/Carbon lithium-ion batteries at subzero ambient temperatures. *J. Power Sources* **2019**, *418*, 61–73. [[CrossRef](#)]

52. Hendricks, C.; Williard, N.; Mathew, S.; Pecht, M. A failure modes, mechanisms, and effects analysis (FMMEA) of lithium-ion batteries. *J. Power Sources* **2015**, *297*, 113–120. [[CrossRef](#)]
53. Ebner, M.; Marone, F.; Stampanoni, M.; Wood, V. Visualization and quantification of electrochemical and mechanical degradation in Li ion batteries. *Science* **2013**, *342*, 716–720. [[CrossRef](#)] [[PubMed](#)]
54. McGrogan, F.P.; Raja, S.N.; Chiang, Y.-M.; Van Vliet, K.J. Electrochemomechanical Fatigue: Decoupling Mechanisms of Fracture-Induced Performance Degradation in  $\text{Li}_x\text{Mn}_2\text{O}_4$ . *J. Electrochem. Soc.* **2018**, *165*, A2458–A2466. [[CrossRef](#)]
55. Müller, S.; Pietsch, P.; Brandt, B.-E.; Baade, P.; De Andrade, V.; De Carlo, F.; Wood, V. Quantification and modeling of mechanical degradation in lithium-ion batteries based on nanoscale imaging. *Nat. Commun.* **2018**, *9*, 2340. [[CrossRef](#)]
56. Xu, R.; Yang, Y.; Yin, F.; Liu, P.; Cloetens, P.; Liu, Y.; Lin, F.; Zhao, K. Heterogeneous damage in Li-ion batteries: Experimental analysis and theoretical modeling. *J. Mech. Phys. Solids* **2019**, *129*, 160–183. [[CrossRef](#)]
57. Newman, J.; Thomas, K.E.; Hafezi, H.; Wheeler, D.R. Modeling of lithium-ion batteries. *J. Power Sources* **2003**, *119–121*, 838–843. [[CrossRef](#)]
58. Balakrishnan, P.; Ramesh, R.; Kumar, T.P. Safety mechanisms in lithium-ion batteries. *J. Power Sources* **2006**, *155*, 401–414. [[CrossRef](#)]
59. du Pasquier, A.; Blyr, A.; Cressent, A.; Lenain, C.; Amatucci, G.; Tarascon, J. An update on the high temperature ageing mechanism in  $\text{LiMn}_2\text{O}_4$ -based Li-ion cells. *J. Power Sources* **1999**, *81–82*, 54–59. [[CrossRef](#)]
60. Buchberger, I.; Seidlmayer, S.; Pokharel, A.; Piana, M.; Hattendorff, J.; Kudejova, P.; Gilles, R.; Gasteiger, H.A. Aging Analysis of Graphite/LiNi 1/3 Mn 1/3 Co 1/3 O 2 Cells Using XRD, PGAA, and AC Impedance. *J. Electrochem. Soc.* **2015**, *162*, A2737–A2746. [[CrossRef](#)]
61. Du Pasquier, A.; Huang, C.; Spitler, T. Nano  $\text{Li}_4\text{Ti}_5\text{O}_{12}$ - $\text{LiMn}_2\text{O}_4$  batteries with high power capability and improved cycle-life. *J. Power Sources* **2009**, *186*, 508–514. [[CrossRef](#)]
62. Wohlfahrt-Mehrens, M.; Vogler, C.; Garche, J. Aging mechanisms of lithium cathode materials. *J. Power Sources* **2004**, *127*, 58–64. [[CrossRef](#)]
63. Gummow, R.; de Kock, A.; Thackeray, M. Improved capacity retention in rechargeable 4 V lithium/lithium-manganese oxide (spinel) cells. *Solid State Ionics* **1994**, *69*, 59–67. [[CrossRef](#)]
64. Li, X.; Xu, Y.; Wang, C. Suppression of Jahn–Teller distortion of spinel  $\text{LiMn}_2\text{O}_4$  cathode. *J. Alloys Compd.* **2009**, *479*, 310–313. [[CrossRef](#)]
65. Chung, K.Y.; Kim, K.-B. Investigations into capacity fading as a result of a Jahn–Teller distortion in 4V  $\text{LiMn}_2\text{O}_4$  thin film electrodes. *Electrochim. Acta* **2004**, *49*, 3327–3337. [[CrossRef](#)]
66. Li, D.; Li, H.; Danilov, D.; Gao, L.; Zhou, J.; Eichel, R.-A.; Yang, Y.; Notten, P.H. Temperature-dependent cycling performance and ageing mechanisms of C6/LiNi1/3Mn1/3Co1/3O2 batteries. *J. Power Sources* **2018**, *396*, 444–452. [[CrossRef](#)]
67. Komaba, S.; Kaplan, B.; Ohtsuka, T.; Kataoka, Y.; Kumagai, N.; Groult, H. Inorganic electrolyte additives to suppress the degradation of graphite anodes by dissolved Mn(II) for lithium-ion batteries. *J. Power Sources* **2003**, *119–121*, 378–382. [[CrossRef](#)]
68. Choa, J.; Thackeray, M.M. Structural Changes of  $\text{LiMn}_2\text{O}_4$  Spinel Electrodes during Electrochemical Cycling. *J. Electrochem. Soc.* **1999**, *146*, 3577–3581. [[CrossRef](#)]
69. Blyr, A.; Sigala, C.; Amatucci, G.; Guyomard, D.; Chabre, Y.; Tarascon, J. Self-Discharge of  $\text{LiMn}_2\text{O}_4/\text{C}$  Li-Ion Cells in Their Discharged State: Understanding by Means of Three-Electrode Measurements. *J. Electrochem. Soc.* **1998**, *145*, 194–209. [[CrossRef](#)]
70. Meissner, E.; Richter, G. The challenge to the automotive battery industry: The battery has to become an increasingly integrated component within the vehicle electric power system. *J. Power Sources* **2005**, *144*, 438–460. [[CrossRef](#)]
71. Erdinc, O.; Vural, B.; Uzunoglu, M. A dynamic lithium-ion battery model considering the effects of temperature and capacity fading. In Proceedings of the 2009 International Conference on Clean Electrical Power, ICCEP 2009, Capri, Italy, 9–11 June 2009; pp. 383–386. [[CrossRef](#)]
72. Bögel, W.; Büchel, J.P.; Katz, H. Real-life EV battery cycling on the test bench. *J. Power Sources* **1998**, *72*, 37–42. [[CrossRef](#)]
73. Wright, R.; Motloch, C.; Belt, J.; Christophersen, J.; Ho, C.; Richardson, R.; Bloom, I.; Jones, S.; Battaglia, V.; Henriksen, G.; et al. Calendar- and cycle-life studies of advanced technology development program generation 1 lithium-ion batteries. *J. Power Sources* **2002**, *110*, 445–470. [[CrossRef](#)]
74. Ohue, K.; Utsunomiya, T.; Hatozaki, O.; Yoshimoto, N.; Egashira, M.; Morita, M. Self-discharge behavior of polyacenic semiconductor and graphite negative electrodes for lithium-ion batteries. *J. Power Sources* **2011**, *196*, 3604–3610. [[CrossRef](#)]
75. Bashash, S.; Moura, S.J.; Forman, J.C.; Fathy, H.K. Plug-in hybrid electric vehicle charge pattern optimization for energy cost and battery longevity. *J. Power Sources* **2011**, *196*, 541–549. [[CrossRef](#)]
76. Schimpe, M.; von Kuepach, M.E.; Naumann, M.; Hesse, H.C.; Smith, K.; Jossen, A. Comprehensive Modeling of Temperature-Dependent Degradation Mechanisms in Lithium Iron Phosphate Batteries. *J. Electrochem. Soc.* **2018**, *165*, A181–A193. [[CrossRef](#)]
77. Kötz, R.; Ruch, P.; Cericola, D. Aging and failure mode of electrochemical double layer capacitors during accelerated constant load tests. *J. Power Sources* **2010**, *195*, 923–928. [[CrossRef](#)]
78. Danzer, M.; Liebau, V.; Maglia, F. Aging of lithium-ion batteries for electric vehicles. In *Advances in Battery Technologies for Electric Vehicles*; Woodhead Publishing: Sawston, UK, 2015; pp. 359–387. [[CrossRef](#)]
79. Bloom, I.; Cole, B.; Sohn, J.; Jones, S.; Polzin, E.; Battaglia, V.; Henriksen, G.; Motloch, C.; Richardson, R.; Unkelhaeuser, T.; et al. An accelerated calendar and cycle life study of Li-ion cells. *J. Power Sources* **2001**, *101*, 238–247. [[CrossRef](#)]

80. Ramadass, P.; Haran, B.; White, R.; Popov, B.N. Mathematical modeling of the capacity fade of Li-ion cells. *J. Power Sources* **2003**, *123*, 230–240. [[CrossRef](#)]
81. Kim, I.-S. Nonlinear state of charge estimator for hybrid electric vehicle battery. *IEEE Trans. Power Electron.* **2008**, *23*, 2027–2034. [[CrossRef](#)]
82. Snihir, I.; Rey, W.; Verbitskiy, E.; Belfadhel-Ayeb, A.; Notten, P.H. Battery open-circuit voltage estimation by a method of statistical analysis. *J. Power Sources* **2006**, *159*, 1484–1487. [[CrossRef](#)]
83. Li, M. Li-ion dynamics and state of charge estimation. *Renew. Energy* **2017**, *100*, 44–52. [[CrossRef](#)]
84. Hu, X.; Li, S.; Peng, H. A comparative study of equivalent circuit models for Li-ion batteries. *J. Power Sources* **2012**, *198*, 359–367. [[CrossRef](#)]
85. Speltino, C.; Di Domenico, D.; Fiengo, G.; Stefanopoulou, A. Comparison of reduced order lithium-ion battery models for control applications. In Proceedings of the IEEE Conference on Decision and Control, Shanghai, China, 15–18 December 2009; pp. 3276–3281. [[CrossRef](#)]
86. Di Domenico, D.; Fiengo, G.; Stefanopoulou, A. Lithium-ion Battery state of charge estimation with a Kalman filter based on a electrochemical model. In Proceedings of the IEEE International Conference on Control Applications, San Antonio, TX, USA, 3–5 September 2008; pp. 702–707. [[CrossRef](#)]
87. Gu, W.B.; Wang, C.Y. Thermal-Electrochemical Modeling of Battery Systems. *J. Electrochem. Soc.* **2000**, *147*, 2910–2922. [[CrossRef](#)]
88. Wang, Q.; Wang, J.; Zhao, P.; Kang, J.; Yan, F.; Du, C. Correlation between the model accuracy and model-based SOC estimation. *Electrochim. Acta* **2017**, *228*, 146–159. [[CrossRef](#)]
89. Rivera-Barrera, J.P.; Muñoz-Galeano, N.; Sarmiento-Maldonado, H.O. SoC Estimation for Lithium-ion Batteries: Review and Future Challenges. *Electronics* **2017**, *6*, 102. [[CrossRef](#)]
90. Chaoui, H.; Ibe-Ekeocha, C.C.; Gualous, H. Aging prediction and state of charge estimation of a LiFePO<sub>4</sub> battery using input time-delayed neural networks. *Electr. Power Syst. Res.* **2017**, *146*, 189–197. [[CrossRef](#)]
91. Zou, C.; Manzie, C.; Nestic, D. A Framework for Simplification of PDE-Based Lithium-Ion Battery Models. *IEEE Trans. Control Syst. Technol.* **2016**, *24*, 1594–1609. [[CrossRef](#)]
92. Bartlett, A.; Marcicki, J.; Onori, S.; Rizzoni, G.; Yang, X.G.; Miller, T. Electrochemical Model-Based State of Charge and Capacity Estimation for a Composite Electrode Lithium-Ion Battery. *IEEE Trans. Control Syst. Technol.* **2016**, *24*, 384–399. [[CrossRef](#)]
93. Ma, Z.; Xie, Z.; Wang, Y.; Zhang, P.; Pan, Y.; Zhou, Y.; Lu, C. Failure modes of hollow core-shell structural active materials during the lithiation–delithiation process. *J. Power Sources* **2015**, *290*, 114–122. [[CrossRef](#)]
94. Jin, X.; Duan, X.; Jiang, W.; Wang, Y.; Zou, Y.; Lei, W.; Sun, L.; Ma, Z. Structural design of a composite board/heat pipe based on the coupled electro-chemical-thermal model in battery thermal management system. *Energy* **2021**, *216*, 119234. [[CrossRef](#)]
95. Duan, X.; Jiang, W.; Zou, Y.; Lei, W.; Ma, Z. A coupled electrochemical–thermal–mechanical model for spiral-wound Li-ion batteries. *J. Mater. Sci.* **2018**, *53*, 10987–11001. [[CrossRef](#)]
96. Ma, Z.; Wu, H.; Wang, Y.; Pan, Y.; Lu, C. An electrochemical-irradiated plasticity model for metallic electrodes in lithium-ion batteries. *Int. J. Plast.* **2017**, *88*, 188–203. [[CrossRef](#)]
97. Yi, S.; Zorzi, M. Robust fixed-lag smoothing under model perturbations. *J. Frankl. Inst.* **2023**, *360*, 458–483. [[CrossRef](#)]
98. El Mejdoubi, A.; Oukaour, A.; Chaoui, H.; Gualous, H.; Sabor, J.; Slamani, Y. State-of-Charge and State-of-Health Lithium-Ion Batteries’ Diagnosis According to Surface Temperature Variation. *IEEE Trans. Ind. Electron.* **2016**, *63*, 2391–2402. [[CrossRef](#)]
99. Zhang, C.; Li, K.; Deng, J.; Song, S. Improved Realtime State-of-Charge Estimation of LiFePO<sub>4</sub> Battery Based on a Novel Thermoelectric Model. *IEEE Trans. Ind. Electron.* **2017**, *64*, 654–663. [[CrossRef](#)]
100. He, H.; Xiong, R.; Zhang, X.; Sun, F.; Fan, J. State-of-charge estimation of the lithium-ion battery using an adaptive extended Kalman filter based on an improved thevenin model. *IEEE Trans. Veh. Technol.* **2011**, *60*, 1461–1469. [[CrossRef](#)]
101. Tian, Y.; Xia, B.; Sun, W.; Xu, Z.; Zheng, W. A modified model based state of charge estimation of power lithium-ion batteries using unscented Kalman filter. *J. Power Sources* **2014**, *270*, 619–626. [[CrossRef](#)]
102. Peng, S.; Chen, C.; Shi, H.; Yao, Z. State of charge estimation of battery energy storage systems based on adaptive unscented Kalman filter with a noise statistics estimator. *IEEE Access* **2017**, *5*, 13202–13212. [[CrossRef](#)]
103. He, W.; Williard, N.; Chen, C.; Pecht, M. State of charge estimation for electric vehicle batteries using unscented kalman filtering. *Microelectron. Reliab.* **2013**, *53*, 840–847. [[CrossRef](#)]
104. Sun, F.; Hu, X.; Zou, Y.; Li, S. Adaptive unscented Kalman filtering for state of charge estimation of a lithium-ion battery for electric vehicles. *Energy* **2011**, *36*, 3531–3540. [[CrossRef](#)]
105. Du, J.; Liu, Z.; Wang, Y. State of charge estimation for Li-ion battery based on model from extreme learning machine. *Control Eng. Pract.* **2014**, *26*, 11–19. [[CrossRef](#)]
106. He, Z.; Liu, Y.; Gao, M.; Wang, C. A joint model and SOC estimation method for lithium battery based on the sigma point KF. In Proceedings of the 2012 IEEE Transportation Electrification Conference and Expo, ITEC 2012, Dearborn, MI, USA, 18–20 June 2012. [[CrossRef](#)]
107. Barillas, J.K.; Li, J.; Günther, C.; Danzer, M.A. A comparative study and validation of state estimation algorithms for Li-ion batteries in battery management systems. *Appl. Energy* **2015**, *155*, 455–462. [[CrossRef](#)]
108. Xiong, R.; Yu, Q.; Wang, L.Y.; Lin, C. A novel method to obtain the open circuit voltage for the state of charge of lithium ion batteries in electric vehicles by using H infinity filter. *Appl. Energy* **2017**, *207*, 346–353. [[CrossRef](#)]



109. Yu, Q.; Xiong, R.; Lin, C. Online Estimation of State-of-charge Based on the H infinity and Unscented Kalman Filters for Lithium Ion Batteries. *Energy Procedia* **2017**, *105*, 2791–2796. [[CrossRef](#)]
110. Eddahech, A.; Briat, O.; Vinassa, J. Adaptive voltage estimation for EV Li-ion cell based on artificial neural networks state-of-charge meter. In Proceedings of the IEEE International Symposium on Industrial Electronics, Hangzhou, China, 28–31 May 2012; pp. 1318–1324. [[CrossRef](#)]
111. Sánchez, L.; Couso, I.; Viera, J.C. Online SOC estimation of Li-FePO<sub>4</sub> batteries through a new fuzzy rule-based recursive filter with feedback of the heat flow rate. In Proceedings of the 2014 IEEE Vehicle Power and Propulsion Conference, VPPC 2014, Coimbra, Portugal, 27–30 October 2014. [[CrossRef](#)]
112. Li, I.-H.; Wang, W.-Y.; Su, S.-F.; Lee, Y.-S. A merged fuzzy neural network and its applications in battery state-of-charge estimation. *IEEE Trans. Energy Convers.* **2007**, *22*, 697–708. [[CrossRef](#)]
113. Chau, K.; Wu, K.; Chan, C. A new battery capacity indicator for lithium-ion battery powered electric vehicles using adaptive neuro-fuzzy inference system. *Energy Convers. Manag.* **2004**, *45*, 1681–1692. [[CrossRef](#)]
114. Awadallah, M.A.; Venkatesh, B. Accuracy improvement of SOC estimation in lithium-ion batteries. *J. Energy Storage* **2016**, *6*, 95–104. [[CrossRef](#)]
115. Yang, F.; Xing, Y.; Wang, D.; Tsui, K.-L. A comparative study of three model-based algorithms for estimating state-of-charge of lithium-ion batteries under a new combined dynamic loading profile. *Appl. Energy* **2016**, *164*, 387–399. [[CrossRef](#)]
116. Dai, H.; Guo, P.; Wei, X.; Sun, Z.; Wang, J. ANFIS (adaptive neuro-fuzzy inference system) based online SOC (State of Charge) correction considering cell divergence for the EV (electric vehicle) traction batteries. *Energy* **2015**, *80*, 350–360. [[CrossRef](#)]
117. Fotouhi, A.; Propp, K.; Auger, D.J. Electric vehicle battery model identification and state of charge estimation in real world driving cycles. In Proceedings of the 2015 7th Computer Science and Electronic Engineering Conference, CEEC 2015—Conference Proceedings, Colchester, UK, 24–25 September 2015; pp. 243–248. [[CrossRef](#)]
118. Antón, J.C.Á.; Nieto, P.J.G.; de Cos Juez, F.J.; Lasheras, F.S.; Vega, M.G.; Gutiérrez, M.N.R. Battery state-of-charge estimator using the SVM technique. *Appl. Math. Model.* **2013**, *37*, 6244–6253. [[CrossRef](#)]
119. Wu, X.; Mi, L.; Tan, W.; Qin, J.L.; Na Zhao, M. State of Charge (SOC) Estimation of Ni-MH Battery Based on Least Square Support Vector Machines. *Adv. Mater. Res.* **2011**, *211–212*, 1204–1209. [[CrossRef](#)]
120. He, W.; Williard, N.; Chen, C.; Pecht, M. State of charge estimation for Li-ion batteries using neural network modeling and unscented Kalman filter-based error cancellation. *Int. J. Electr. Power Energy Syst.* **2014**, *62*, 783–791. [[CrossRef](#)]
121. Chen, Z.; Qiu, S.; Masrur, M.; Murphey, Y.L. Battery state of charge estimation based on a combined model of extended Kalman filter and neural networks. In Proceedings of the International Joint Conference on Neural Networks, San Jose, CA, USA, 31 July–5 August 2011; pp. 2156–2163. [[CrossRef](#)]
122. Li, Y.; Wang, C.; Gong, J. A combination Kalman filter approach for State of Charge estimation of lithium-ion battery considering model uncertainty. *Energy* **2016**, *109*, 933–946. [[CrossRef](#)]
123. Xia, B.; Chen, C.; Tian, Y.; Sun, W.; Xu, Z.; Zheng, W. A novel method for state of charge estimation of lithium-ion batteries using a nonlinear observer. *J. Power Sources* **2014**, *270*, 359–366. [[CrossRef](#)]
124. Han, H.; Xu, H.; Yuan, Z.; Zhao, Y. State of Charge estimation of Li-ion battery in EVs based on second-order sliding mode observer. In Proceedings of the IEEE Transportation Electrification Conference and Expo, ITEC Asia-Pacific 2014—Conference Proceedings, Beijing, China, 31 August–3 September 2014. [[CrossRef](#)]
125. Anton, J.C.A.; Nieto, P.J.G.; Gonzalo, E.G.; Perez, J.C.V.; Vega, M.G.; Viejo, C.B. A New Predictive Model for the State-of-Charge of a High-Power Lithium-Ion Cell Based on a PSO-Optimized Multivariate Adaptive Regression Spline Approach. *IEEE Trans. Veh. Technol.* **2016**, *65*, 4197–4208. [[CrossRef](#)]
126. Ranjbar, A.H.; Banaei, A.; Khoobroo, A.; Fahimi, B. Online estimation of state of charge in li-imi batteries using impulse response concept. *IEEE Trans. Smart Grid* **2012**, *3*, 360–367. [[CrossRef](#)]
127. Wang, L.; Wang, L.; Li, Y. A novel state-of-charge estimation algorithm of EV battery based on bilinear interpolation. In Proceedings of the 2013 9th IEEE Vehicle Power and Propulsion Conference, IEEE VPPC 2013, Beijing, China, 15–18 October 2013; pp. 26–29. [[CrossRef](#)]
128. Ge, M.-F.; Liu, Y.; Jiang, X.; Liu, J. A review on state of health estimations and remaining useful life prognostics of lithium-ion batteries. *Measurement* **2021**, *174*, 109057. [[CrossRef](#)]
129. Shahjalal, M.; Roy, P.K.; Shams, T.; Fly, A.; Chowdhury, J.I.; Ahmed, R.; Liu, K. A review on second-life of Li-ion batteries: Prospects, challenges, and issues. *Energy* **2022**, *241*, 122881. [[CrossRef](#)]
130. Zhang, Y.; Song, W.; Lin, S.; Feng, Z. A novel model of the initial state of charge estimation for LiFePO<sub>4</sub> batteries. *J. Power Sources* **2014**, *248*, 1028–1033. [[CrossRef](#)]
131. Zhang, C.; Jiang, J.; Zhang, L.; Liu, S.; Wang, L.; Loh, P.C. A Generalized SOC-OCV Model for Lithium-Ion Batteries and the SOC Estimation for LNMCO Battery. *Energies* **2016**, *9*, 900. [[CrossRef](#)]
132. Wang, X.; Wei, X.; Dai, H. Estimation of state of health of lithium-ion batteries based on charge transfer resistance considering different temperature and state of charge. *J. Energy Storage* **2019**, *21*, 618–631. [[CrossRef](#)]
133. Yatsui, M.W.; Bai, H. Kalman filter based state-of-charge estimation for lithium-ion batteries in hybrid electric vehicles using pulse charging. In Proceedings of the 2011 IEEE Vehicle Power and Propulsion Conference, VPPC 2011, Chicago, IL, USA, 6–9 September 2011. [[CrossRef](#)]

134. Chen, Z.; Fu, Y.; Mi, C.C. State of charge estimation of lithium-ion batteries in electric drive vehicles using extended Kalman filtering. *IEEE Trans. Veh. Technol.* **2012**, *62*, 1020–1030. [CrossRef]
135. Xiong, R.; He, H.; Sun, F.; Zhao, K. Evaluation on state of charge estimation of batteries with adaptive extended Kalman filter by experiment approach. *IEEE Trans. Veh. Technol.* **2013**, *62*, 108–117. [CrossRef]
136. Plett, G.L. Sigma-point Kalman filtering for battery management systems of LiPB-based HEV battery packs. Part 1: Introduction and state estimation. *J. Power Sources* **2006**, *161*, 1356–1368. [CrossRef]
137. Yang, J.; Xia, B.; Huang, W.; Fu, Y.; Mi, C. Online state-of-health estimation for lithium-ion batteries using constant-voltage charging current analysis. *Appl. Energy* **2018**, *212*, 1589–1600. [CrossRef]
138. He, W.; Pecht, M.; Flynn, D.; Dinmohammadi, F. A Physics-Based Electrochemical Model for Lithium-Ion Battery State-of-Charge Estimation Solved by an Optimised Projection-Based Method and Moving-Window Filtering. *Energies* **2018**, *11*, 2120. [CrossRef]
139. Li, P.; Zhang, Z.; Xiong, Q.; Ding, B.; Hou, J.; Luo, D.; Rong, Y.; Li, S. State-of-health estimation and remaining useful life prediction for the lithium-ion battery based on a variant long short term memory neural network. *J. Power Sources* **2020**, *459*, 228069. [CrossRef]
140. Zhang, W.; Li, X.; Li, X. Deep learning-based prognostic approach for lithium-ion batteries with adaptive time-series prediction and on-line validation. *Measurement* **2020**, *164*, 108052. [CrossRef]
141. Salkind, A.J.; Fennie, C.; Singh, P.; Atwater, T.; E Reisner, D. Determination of state-of-charge and state-of-health of batteries by fuzzy logic methodology. *J. Power Sources* **1999**, *80*, 293–300. [CrossRef]
142. Gao, W.; Zheng, Y.; Ouyang, M.; Li, J.; Lai, X.; Hu, X. Micro-short-circuit diagnosis for series-connected lithium-ion battery packs using mean-difference model. *IEEE Trans. Ind. Electron.* **2019**, *66*, 2132–2142. [CrossRef]
143. Li, H.; Pan, D.; Chen, C.L.P. Intelligent prognostics for battery health monitoring using the mean entropy and relevance vector machine. *IEEE Trans. Syst. Man Cybern. Syst.* **2014**, *44*, 851–862. [CrossRef]
144. Meng, J.; Cai, L.; Luo, G.; Stroe, D.-I.; Teodorescu, R. Lithium-ion battery state of health estimation with short-term current pulse test and support vector machine. *Microelectron. Reliab.* **2018**, *88–90*, 1216–1220. [CrossRef]
145. Xu, J.; Cao, B.; Chen, Z.; Zou, Z. An online state of charge estimation method with reduced prior battery testing information. *Int. J. Electr. Power Energy Syst.* **2014**, *63*, 178–184. [CrossRef]
146. Zhang, Y.; Zhang, C.; Zhang, X. State-of-charge estimation of the lithium-ion battery system with time-varying parameter for hybrid electric vehicles. *IET Control Theory Appl.* **2014**, *8*, 160–167. [CrossRef]
147. Dong, G.; Chen, Z.; Wei, J.; Ling, Q. Battery health prognosis using brownian motion modeling and particle filtering. *IEEE Trans. Ind. Electron.* **2018**, *65*, 8646–8655. [CrossRef]
148. Xiong, R.; Tian, J.; Mu, H.; Wang, C. A systematic model-based degradation behavior recognition and health monitoring method for lithium-ion batteries. *Appl. Energy* **2017**, *207*, 372–383. [CrossRef]
149. State of Health—Wikipedia. Available online: [https://en.wikipedia.org/wiki/State\\_of\\_health](https://en.wikipedia.org/wiki/State_of_health) (accessed on 7 September 2023).
150. Liu, K.; Li, K.; Peng, Q.; Zhang, C. A brief review on key technologies in the battery management system of electric vehicles. *Front. Mech. Eng.* **2019**, *14*, 47–64. [CrossRef]
151. Chiang, Y.-H.; Sean, W.-Y.; Ke, J.-C. Online estimation of internal resistance and open-circuit voltage of lithium-ion batteries in electric vehicles. *J. Power Sources* **2011**, *196*, 3921–3932. [CrossRef]
152. Wang, Z.; Feng, G.; Zhen, D.; Gu, F.; Ball, A. A review on online state of charge and state of health estimation for lithium-ion batteries in electric vehicles. *Energy Rep.* **2021**, *7*, 5141–5161. [CrossRef]
153. Nuhic, A.; Terzimehic, T.; Soczka-Guth, T.; Buchholz, M.; Dietmayer, K. Health diagnosis and remaining useful life prognostics of lithium-ion batteries using data-driven methods. *J. Power Sources* **2013**, *239*, 680–688. [CrossRef]
154. Hu, X.; Feng, F.; Liu, K.; Zhang, L.; Xie, J.; Liu, B. State estimation for advanced battery management: Key challenges and future trends. *Renew. Sustain. Energy Rev.* **2019**, *114*, 109334. [CrossRef]
155. Wang, D.; Kong, J.-Z.; Yang, F.; Zhao, Y.; Tsui, K.-L. Battery prognostics at different operating conditions. *Measurement* **2020**, *151*, 107182. [CrossRef]
156. Hu, C.; Ye, H.; Jain, G.; Schmidt, C. Remaining useful life assessment of lithium-ion batteries in implantable medical devices. *J. Power Sources* **2018**, *375*, 118–130. [CrossRef]
157. Bian, X.; Liu, L.; Yan, J.; Zou, Z.; Zhao, R. An open circuit voltage-based model for state-of-health estimation of lithium-ion batteries: Model development and validation. *J. Power Sources* **2020**, *448*, 227401. [CrossRef]
158. Xiong, R.; Zhang, Y.; He, H.; Zhou, X.; Pecht, M.G. A double-scale, particle-filtering, energy state prediction algorithm for lithium-ion batteries. *IEEE Trans. Ind. Electron.* **2017**, *65*, 1526–1538. [CrossRef]
159. Tan, X.; Zhan, D.; Lyu, P.; Rao, J.; Fan, Y. Online state-of-health estimation of lithium-ion battery based on dynamic parameter identification at multi timescale and support vector regression. *J. Power Sources* **2021**, *484*, 229233. [CrossRef]
160. He, H.; Xiong, R.; Guo, H. Online estimation of model parameters and state-of-charge of LiFePO<sub>4</sub> batteries in electric vehicles. *Appl. Energy* **2012**, *89*, 413–420. [CrossRef]
161. Andre, D.; Meiler, M.; Steiner, K.; Wimmer, C.; Soczka-Guth, T.; Sauer, D. Characterization of high-power lithium-ion batteries by electrochemical impedance spectroscopy. I. Experimental investigation. *J. Power Sources* **2011**, *196*, 5334–5341. [CrossRef]
162. Galeotti, M.; Cinà, L.; Giammanco, C.; Cordiner, S.; Di Carlo, A. Performance analysis and SOH (state of health) evaluation of lithium polymer batteries through electrochemical impedance spectroscopy. *Energy* **2015**, *89*, 678–686. [CrossRef]



163. Smith, K.A.; Rahn, C.D.; Wang, C.-Y. Model-based electrochemical estimation and constraint management for pulse operation of lithium ion batteries. *IEEE Trans. Control Syst. Technol.* **2010**, *18*, 654–663. [[CrossRef](#)]
164. Weng, C.; Cui, Y.; Sun, J.; Peng, H. On-board state of health monitoring of lithium-ion batteries using incremental capacity analysis with support vector regression. *J. Power Sources* **2013**, *235*, 36–44. [[CrossRef](#)]
165. Li, Y.; Abdel-Monem, M.; Gopalakrishnan, R.; Berecibar, M.; Nanini-Maury, E.; Omar, N.; van den Bossche, P.; Van Mierlo, J. A quick on-line state of health estimation method for Li-ion battery with incremental capacity curves processed by Gaussian filter. *J. Power Sources* **2018**, *373*, 40–53. [[CrossRef](#)]
166. Li, X.; Wang, Z.; Zhang, L.; Zou, C.; Dorrell, D.D. State-of-health estimation for Li-ion batteries by combing the incremental capacity analysis method with grey relational analysis. *J. Power Sources* **2019**, *410–411*, 106–114. [[CrossRef](#)]
167. Wang, Z.; Ma, J.; Zhang, L. State-of-Health Estimation for Lithium-Ion Batteries Based on the Multi-Island Genetic Algorithm and the Gaussian Process Regression. *IEEE Access* **2017**, *5*, 21286–21295. [[CrossRef](#)]
168. Shibagaki, T.; Merla, Y.; Offer, G.J. Tracking degradation in lithium iron phosphate batteries using differential thermal voltammetry. *J. Power Sources* **2018**, *374*, 188–195. [[CrossRef](#)]
169. Xiong, R.; Ma, S.; Li, H.; Sun, F.; Li, J. Toward a Safer Battery Management System: A Critical Review on Diagnosis and Prognosis of Battery Short Circuit. *iScience* **2020**, *23*, 101010. [[CrossRef](#)] [[PubMed](#)]
170. Bloom, I.; Jansen, A.N.; Abraham, D.P.; Knuth, J.; Jones, S.A.; Battaglia, V.S.; Henriksen, G.L. Differential voltage analyses of high-power, lithium-ion cells: 1. Technique and application. *J. Power Sources* **2005**, *139*, 295–303. [[CrossRef](#)]
171. Schiffer, Z.J.; Cannarella, J.; Arnold, C.B. Strain derivatives for practical charge rate characterization of lithium ion electrodes. *J. Electrochem. Soc.* **2016**, *163*, A427–A433. [[CrossRef](#)]
172. Merla, Y.; Wu, B.; Yufit, V.; Brandon, N.P.; Martinez-Botas, R.F.; Offer, G.J. Novel application of differential thermal voltammetry as an in-depth state-of-health diagnosis method for lithium-ion batteries. *J. Power Sources* **2016**, *307*, 308–319. [[CrossRef](#)]
173. Merla, Y.; Wu, B.; Yufit, V.; Brandon, N.P.; Martinez-Botas, R.F.; Offer, G.J. Extending battery life: A low-cost practical diagnostic technique for lithium-ion batteries. *J. Power Sources* **2016**, *331*, 224–231. [[CrossRef](#)]
174. Cannarella, J.; Arnold, C.B. State of health and charge measurements in lithium-ion batteries using mechanical stress. *J. Power Sources* **2014**, *269*, 7–14. [[CrossRef](#)]
175. Sommer, L.W.; Raghavan, A.; Kiesel, P.; Saha, B.; Schwartz, J.; Lochbaum, A.; Ganguli, A.; Bae, C.-J.; Alamgir, M. Monitoring of Intercalation Stages in Lithium-Ion Cells over Charge-Discharge Cycles with Fiber Optic Sensors. *J. Electrochem. Soc.* **2015**, *162*, A2664–A2669. [[CrossRef](#)]
176. Oh, K.-Y.; Siegel, J.B.; Secondo, L.; Kim, S.U.; Samad, N.A.; Qin, J.; Anderson, D.; Garikipati, K.; Knobloch, A.; Epureanu, B.I.; et al. Rate dependence of swelling in lithium-ion cells. *J. Power Sources* **2014**, *267*, 197–202. [[CrossRef](#)]
177. Juang, L.W. *Online Battery Monitoring for State-of-Charge and Power Capability Prediction*; University of Wisconsin: Madison, WI, USA, 2010.
178. Lukic, S.; Emadi, A. Charging ahead. *IEEE Ind. Electron. Mag.* **2008**, *2*, 22–31. [[CrossRef](#)]
179. Plett, G.L. *Battery Management Systems. Volume II, Equivalent-Circuit Methods*. Artech: Norwood, MA, USA, 2015.
180. Balagopal, B.; Chow, M.-Y. The state of the art approaches to estimate the state of health (SOH) and state of function (SOF) of lithium ion batteries. In Proceedings of the 2015 IEEE International Conference on Industrial Informatics, INDIN 2015, Cambridge, UK, 22–24 July 2015; Institute of Electrical and Electronics Engineers Inc.: Piscataway, NJ, USA, 2015; pp. 1302–1307. [[CrossRef](#)]
181. Lin, X.; Stefanopoulou, A.G.; Perez, H.E.; Siegel, J.B.; Li, Y.; Anderson, R.D. Quadruple adaptive observer of the core temperature in cylindrical Li-ion batteries and their health monitoring. In Proceedings of the 2012 American Control Conference (ACC), Montreal, QC, Canada, 27–29 June 2012; pp. 578–583. [[CrossRef](#)]
182. Park, S.; Ahn, J.; Kang, T.; Park, S.; Kim, Y.; Cho, I.; Kim, J. Review of state-of-the-art battery state estimation technologies for battery management systems of stationary energy storage systems. *J. Power Electron.* **2020**, *20*, 1526–1540. [[CrossRef](#)]
183. Li, J.; Sun, D.; Jin, X.; Shi, W.; Sun, C. Lithium-ion battery overcharging thermal characteristics analysis and an impedance-based electro-thermal coupled model simulation. *Appl. Energy* **2019**, *254*, 113574. [[CrossRef](#)]
184. Zhang, C.; Li, K.; Deng, J. Real-time estimation of battery internal temperature based on a simplified thermoelectric model. *J. Power Sources* **2016**, *302*, 146–154. [[CrossRef](#)]
185. Zhu, J.; Sun, Z.; Wei, X.; Dai, H. Battery Internal Temperature Estimation for LiFePO<sub>4</sub> Battery Based on Impedance Phase Shift under Operating Conditions. *Energies* **2017**, *10*, 60. [[CrossRef](#)]
186. Farmann, A.; Sauer, D.U. A comprehensive review of on-board State-of-Available-Power prediction techniques for lithium-ion batteries in electric vehicles. *J. Power Sources* **2016**, *329*, 123–137. [[CrossRef](#)]
187. Feng, T.; Yang, L.; Zhao, X.; Zhang, H.; Qiang, J. Online identification of lithium-ion battery parameters based on an improved equivalent-circuit model and its implementation on battery state-of-power prediction. *J. Power Sources* **2015**, *281*, 192–203. [[CrossRef](#)]
188. Burgos-Mellado, C.; Orchard, M.E.; Kazerani, M.; Cárdenas, R.; Sáez, D. Particle-filtering-based estimation of maximum available power state in Lithium-Ion batteries. *Appl. Energy* **2016**, *161*, 349–363. [[CrossRef](#)]
189. Pei, L.; Zhu, C.; Wang, T.; Lu, R.; Chan, C. Online peak power prediction based on a parameter and state estimator for lithium-ion batteries in electric vehicles. *Energy* **2014**, *66*, 766–778. [[CrossRef](#)]
190. Zhou, L.; Lai, X.; Li, B.; Yao, Y.; Yuan, M.; Weng, J.; Zheng, Y. State Estimation Models of Lithium-Ion Batteries for Battery Management System: Status, Challenges, and Future Trends. *Batteries* **2023**, *9*, 131. [[CrossRef](#)]

191. Zhao, J.; Zhu, Y.; Zhang, B.; Liu, M.; Wang, J.; Liu, C.; Hao, X. Review of State Estimation and Remaining Useful Life Prediction Methods for Lithium–Ion Batteries. *Sustainability* **2023**, *15*, 5014. [[CrossRef](#)]
192. Zhao, D.; Li, H.; Zhou, F.; Zhong, Y.; Zhang, G.; Liu, Z.; Hou, J. Research Progress on Data-Driven Methods for Battery States Estimation of Electric Buses. *World Electr. Veh. J.* **2023**, *14*, 145. [[CrossRef](#)]

**Disclaimer/Publisher’s Note:** The statements, opinions and data contained in all publications are solely those of the individual author(s) and contributor(s) and not of MDPI and/or the editor(s). MDPI and/or the editor(s) disclaim responsibility for any injury to people or property resulting from any ideas, methods, instructions or products referred to in the content.